Accepted Manuscript

Journal of the Geological Society

Climatic and tectonic controls on ferroan dolomite formation – insights on Early Miocene Mediterranean anoxia (il-Blata, Malta)

Ray Zammit, D.A. Petrash & O.M. Bialik

DOI: https://doi.org/10.1144/jgs2024-146

To access the most recent version of this article, please click the DOI URL in the line above. When citing this article please include the above DOI.

Received 25 July 2024
Revised 19 December 2024
Accepted 2 January 2025

Supplementary material at https://doi.org/10.6084/m9.figshare.c.7618306

Title

Climatic and tectonic controls on ferroan dolomite formation – insights on Early Miocene Mediterranean anoxia (il-Blata, Malta).

Abbreviated title

Early Miocene Mediterranean iron dolomite

Ray Zammit[1,2 *], D.A. Petrash[3], O.M. Bialik[4,5]

1. School of Earth and Environmental Sciences, Cardiff University, UK.
2. Department of Mathematics and Science Education, The University of Malta, Malta.
3. Department of Environmental Geochemistry and Biogeochemistry, Czech Geological Survey, Prague.
4. Universität Münster, Institut für Geologie und Paläontologie.
5. University of Haifa, Charney School of Marine Sciences, Department of Marine Geosciences.

*Correspondence (zammitr2@cardiff.ac.uk. raymond.zammit@um.edu.mt)

R.Z. 0000-0002-8629-3793

D.A.P. 0000-0001-5039-0543

O.M.B. 0000-0003-1915-7297

Abstract

Records from the Miocene il-Blata section in Malta offer insights into the Central Mediterranean's depositional environments following an Early Miocene restriction of the Mesopotamian Seaway (~20 Ma). Inorganic and organic stable carbon isotope values suggest relatively steady depositional environments, whereas authigenic Fe-dolomite abundances exhibiting substantial $\delta^{18}O$ and $\delta^{13}C$ variations at a sequence-scale indicate dynamic sedimentation conditions leading to differential diagenesis. Petrographically, the dolomitic levels exhibit matrix-selective dolomitisation, occasional silicification and phosphatisation, and textural indicators pointing to subsurface microbial influence which collectively point to complex shallow burial diagenesis. In addition, the presence of framboidal pyrite and gypsum infilling foraminiferal chambers along with the absence of large planktonic foraminifera, suggests the development of paleoenvironmental stress imposed by a density-stratified water column affecting pore waters. Towards the top of the studied succession, a shift from organic to siliceous deposits reflects water column perturbations possibly linked to changes in oceanic circulation associated with a temporary re-opening of the Mesopotamian Seaway. This study not only underscores hydrochemical controls exerted by North African terrigenous fluxes over the Mediterranean, but also highlights the intricate interplay between shifting depositional environments and shallow burial diagenetic processes in shaping the geochemical and textural fabrics of authigenic mineral assemblages.

Introduction

Autochthonous biogenic sedimentation in pelagic and hemi-pelagic realms is considered to be predominantly a mixture of two modes: (1) slow background rain of biogenic debris from the sea surface, and (2) rapid solute influxes associated with blooms in biological productivity (Hüneke & Henrich, 2011). Biogenic productivity is dependent on the availability of nutrients, notably nitrogen, phosphate and silica as well as micronutrients such as iron, which is considered as the master bio-limiting nutrient in marine systems (Emerson, 2016; Jiang et al., 2023). Iron fluxes into open marine settings can be from varying combinations of continental runoff, aeolian input, resuspension of shallow sediments, ice-rafted debris, extra-terrestrial sources, subaerial and submarine volcanism and exhalative hydrothermal input (Boyd & Ellwood, 2010; Emerson, 2016). The provenance of iron into the marine system can vary, with certain fluxes becoming more important than others at different sites and between different ocean basins. It has been shown that some of the modes of ancient oceanic iron delivery affecting paleoproductivity can be controlled by astronomical cycles (Auer et al., 2016; Kocken et al., 2019; Lyu et al., 2023). In more recent geological history, Holocene glacial-interglacial changes in atmospheric CO_2 oscillations have also been linked to the availability of iron for surface ocean productivity, with iron being a key component for phytoplankton-controlled feedbacks in the carbon-cycle (Martin, 1990; Watson et al., 2000).

Neogene and Holocene marine sediments contain significant amounts of dolomite [$CaMg(CO_3)_2$] and related rhombohedral phases comprising the dolomite-ankerite series (Petrash et al., 2017, Liu et al., 2024). Ankerite [$Ca, Fe(CO_3)_2$] *sensu stricto,* is a carbonate mineral in which iron (Fe) completely replaces magnesium (Mg) in the rhombohedral dolomite structure; yet such complete replacement has never been observed in nature. In contrast, kutnohorite [$Ca, Mn (CO_3)_2$], demonstrates that Mg can be fully replaced by manganese (Bridges et al., 2014). Intermediary minerals with a general formula [$Ca(Fe,Mg,Mn)(CO_3)_2$] in which the divalent cations are incorporated in the rhombohedral $\bar{R}3$ structure exist, and are named according to the cation ratio (Bridges et al., 2014, Liu et al., 2024). In this scheme, the dolomite–ankerite series represents a compositional continuum between pure dolomite with a molar ratio of Mg/(Mg+Fe) = 1, and pure ankerite, which has Mg/(Mg+Fe) = 0. The intermediate compositions are termed Fe-dolomite (Mg/(Mg+Fe) ≥ 0.5, or Mg-ankerite (Mg/(Mg+Fe) < 0.5 (Bridges et al., 2014). This series reflects the geochemical conditions of precipitation, with all members maintaining $\bar{R}3$ symmetry. The formation of iron-bearing dolomite is directly influenced by the evolving composition of intermediate diagenetic fluids (Böttcher & Dietzel, 2011; Woods & Garrels, 1992), with the diagenetic realm defined from hundreds of metres to about 2 km burial depths; $T < 100°C$ (Immenhauser, 2022). For example, the iron content of dolomite in the Monterey Formation, which registers maximum diagenetic temperatures of about 45-50°C, achieved at burial depths that do not exceeded 750 m (Eichhubl & Boles, 2000, Bradbury et al., 2015; Isaacs, 1982) appears to increase in zones exhibiting large fluxes of terrigenous material (Burns & Baker, 1987). The reasons for this are (1) the rapid burial of sediment quickly buries reactive iron making it available for incorporation into dolomite formed prior to the onset of sulphate reduction, and (2) high sedimentation rates being associated with large fluxes of terrigenous material which is the main source of iron to the basin. (Burns & Baker, 1987).

Reactive iron-bearing lithologies are usually associated with siliceous deposits, e.g., cherts, with a strong control exerted by inputs of silica from continental weathering (Maliva et al., 2005). Chert nodules are generally thought to form as a series of replacement and void-filling processes within sediments. The exact implications in terms of origin, palaeoceanographic and climatic significance of these deposits remains uncertain (Madsen & Stemmerik, 2010). It has been recently suggested that the removal of silica from seawater and the eventual incorporation into sediment is driven by the redox cycling of iron (Li et al., 2022). In this model, Si is precipitated from seawater in conjunction with iron in the form of Fe(III)-Si gels. These gels get disassociated in anoxic sediments, releasing the Si which gets preserved in sediment (Li et al., 2022). This supports the notion linking iron-redox cycling and chert formation.

In (sub)polar regions the supply of iron through aeolian inputs is well characterized as only a few major rivers are present. The situation in subtropical and tropical regions, however, is more complicated due to the presence of significant river systems. There, the intricate interplay of riverine and aeolian inputs opens the possibility for transient localized oceanic iron excess whose effects in sediment authigenic response are unclear (Boyd & Ellwood, 2010; Jickells & Moore, 2015). The Southern Mediterranean is an ideal place to investigate the effects of iron availability on bioproductivity due to its proximity to the North African landmass, a large source of continental-derived solutes and nutrients, and its enclosed nature (Fig. 1). Moreover, the distant influence of runoff and dust from the relatively arid North African margin allows for a degree of control and differentiation between these sources. It has previously been reported that diagenetic ankerite occurs within the Miocene Globigerina Limestone formation on the Central Mediterranean archipelago of Malta (John et al., 2003). More recent

characterisation of the Globigerina Limestone Formation has revealed the presence of Early Miocene organic-rich carbonate mudstones and overlying chert-bearing deposits (Zammit et al., 2022). The shift from shallow marine phosphorite bearing limestones to these organic-rich and cherty deposits, may represent a response to the temporary closure of Mesopotamian Gateway and the ensuing perturbations in Mediterranean circulation and increased hydroclimatic activity over western North Africa around 20 Ma (Zammit et al., 2022). Therefore, the il-Blata deposits offer an opportunity to investigate the influence of changing hydroclimate over North Africa and the restriction of the Mediterranean basin on Central Mediterranean depositional systems. For this purpose, we elucidate water column processes associated with variability in nutrient fluxes that can exert an authigenic responses in the depositional system. We hypothesize that changes in solute delivery carrying oxides, silica and phosphorus significantly impacted mineral saturation states and dolomite precipitation rates in a mode that induced fabric-preserving dolomitisation. To address these hypotheses, we pose the following research questions: *(1) What are the characteristics and stratigraphic location of diagenetic iron-bearing dolomite in the Maltese outcrops, and how is its formation associated with Mediterranean paleoenvironments driven by North African hydroclimate and changes in ocean circulation? (2) What water column processes can explain the shift from organic facies to cherty facies at the il-Blata section, and how do these diagenetic processes relate to the broader paleoenvironments influenced by North African hydroclimate and ocean circulation changes?*

Geological setting and research context

The Mediterranean Sea (Fig. 1) is considered as a natural laboratory to investigate closely coupled depositional processes driven by tectonic and climatic factors. Its hypersensitivity to these forcing factors is reflected in changes on its geochemistry, sedimentology and stratigraphy, as recorded by fossil variability and depositional cyclicity (Meijer, 2021; Reich et al., 2022). Related changes in water column conditions led to a range of sedimentary rocks from evaporites to organic-rich pelagic sediments being preserved (Casanova-Arenillas et al., 2022; Haq et al., 2020; Meijer, 2021; Roveri et al., 2020; Rutten et al., 1999). The dynamic tectono-climatic evolution of the Mediterranean basin throughout the Miocene has also led to incompleteness of the record. This is particularly problematic during the Early Miocene as demonstrated by the fact that base-Burdigalian and base-Langhian Global Boundary Stratotype Section and Points (GSSPs) have never been established (Gradstein et al., 2020). Several regional unconformities have also been reported across the basin in sections of Middle Miocene age (Cipollari & Cosentino, 1995; Eaton & Robertson, 1993). The almost complete desiccation of the basin during the Messinian Salinity Crisis, at the end of the Miocene also lead to gaps in the stratigraphic record of the region (Haq et al., 2020). Large scale tectonic changes in the Mediterranean occurred during the Miocene (23 Ma to 5.6 Ma) (Rögl, 1999), with formation of a basin in a form that closely resembles the present-day mostly enclosed sea occurring around 14 Ma. Then, the water flow from the Indian Ocean through the Mesopotamian Seaway was completely closed off (Mesopotamian Seaway Restriction event number 2, MSR-2) (Bialik et al., 2019; Zammit et al., 2022). The full extent of oceanographic and environmental changes resulting from the transition from the long-standing (~100 Ma; Barron & Peterson, 1989) low latitude halo-thermal circulation to a strong thermohaline system has not been fully revealed and requires detailed investigation. An enclosed configuration would have promoted the generation of oxygen minimum zones in the Eastern Basin as evidenced by the existence of laminated, dark coloured, sulphur-rich muds often referred to as sapropels (Rohling, 1994). Eastern Mediterranean sapropel deposition reflects hydroclimate and associated fertilisation of surface waters and variability in the activity of the Nile influx to the basin (Rohling, 1994; Rohling et al., 2015).

Mediterranean sapropels seem to have occurred almost periodically since 13.5 Ma, mostly within the Eastern Basin (Rohling et al., 2015). Recent work has revealed records for earlier sapropelic events (~16 Ma) as identified from sedimentary deposits in Cyprus (Bialik et al., 2022; Taylforth et al., 2014). There is also evidence for Mediterranean sapropels occurring within the Western Basin, where they are sometimes referred to as Organic Rich Layers (ORLs) (Anastasakis & Stanley, 1984; Incarbona & Sprovieri, 2020; Pérez-Asensio et al., 2020). These western ORLs from Plio-Pleistocene facies exhibit plausible temporal correlation with the eastern sapropels. However, there are important exceptions, suggesting that different mechanisms may have been at play during the development of low oxygen conditions prone to sapropel deposition (Rohling et al., 2015). The abundant organic matter in the sapropels can be partially degraded diagenetically, resulting in the formation of authigenic carbonates (Leonova et al., 2019; Thomson et al., 2004)

Based solely XRD analyses of the d_{104} distance iron-rich diagenetic carbonates, John et al. (2003) identified ankerite in the Oligo-Miocene Globigerina Limestone Formation outcropping in Malta. Their interpretation is that sedimentary processes linked to those phases and stratigraphic clay mineral variability on the Maltese Islands were controlled by now-extinct North African drainage networks. More recent work has refined the age model for the Globigerina Limestone Formation and has revealed the presence of high sulphur, organic-rich laminated beds occurring within the Early Miocene Middle Globigerina Limestone member (Zammit et al., 2022). These thinly bedded mudstones are conformably capped by cherty mudstones that can be roughly

correlated with siliceous-bearing rock formations occurring over wide areas of North Africa (Ben Yahia et al., 2019; Riahi et al., 2015). Best exposed in the il-Blata outcrop (35°54'00.6"N, 14°19'52.2"E), these mudstones also host a geochemical record of an Early Miocene restriction episode of the Mesopotamian gateway into the Eastern Mediterranean (Mesopotamian Seaway Restriction event number 1, MSR-1 at ~ 20 Ma) (Bialik et al., 2019; Zammit et al., 2022). The il-Blata mudstone sequences are also roughly time-related with intermittent activity of the Fezzan mega lake system in North Africa (Fig. 1) (Drake et al., 2022; Hounslow et al., 2017). Other mega lake systems, such as the Chott system, are known from more recent geological history, but there is scant evidence yet of their existence during the Miocene since sedimentological evidence is likely obscured by sand dunes and desert processes (Drake et al., 2022; Drake et al., 2011).

Using known models that compare the effects on low latitude circulation due to the closure of the Mesopotamian Seaway, it has previously been proposed that land-ocean interactions over western North Africa would have been intensified following the closure of the Seaway (Bialik et al., 2019; de la Vara & Meijer, 2016). It can be reasonably assumed that such an intensification in land-ocean interactions resulted in increased continental runoff onto the Central Mediterranean. This mechanism has been used to explain the shift from low-productivity phosphorite bearing marine limestones to high sedimentation rate mixed carbonate-siliciclastic depositional system containing organic-rich layers found at the il-Blata outcrop in Malta (Zammit et al., 2022). Considering the presence of diagenetically altered limestones, organic-rich mudstone facies, and close temporal association of the seaway restriction, it is instructive to consider what paleoenvironmental changes on the water column were recorded into shallow sediment in the Central Mediterranean at the time. In this context, the Maltese il-Blata outcrop is ideally placed, both temporally and geographically, to assess these phenomena and add to the growing knowledge related to iron-bearing minerals, chert nodule formation, and diagenesis induced through continent-to-ocean dynamics and the regional palaeoceanography of the Early Miocene

Methods

Outcrop sampling

Over 100 samples were collected during field excursions at the il-Blata outcrop along the southern coast of the island of Malta. These samples were obtained from the Globigerina Limestone formation, in particular from the highly weathered, Lower Globigerina Limestone member and the overlying base level of the Middle Globigerina Limestone member. This outcrop has been previously divided into two depositional intervals based on coarseness of the lithology at outcrop (Zammit et al., 2022). Based on sedimentological interpretation at outcrop, Depositional Interval 1 has been divided into three sedimentary packages (I, II, III) and depositional interval 2 into four packages (IV, V, VI, VII) (Fig. 2). This study focuses on samples taken from the fine-grained sequences of depositional interval 2. This interval has previously been interpreted to represent a shift from marine dominated limestones of depositional interval 1 to a mixture of marine and terrestrial influenced deposits indicative of changes in hydroclimatic activity in the region during the Early Miocene (Zammit et al., 2022)

Mineralogy and Geochemistry

Mineral content analyses were carried out on selected samples using a Rigaku MiniFlex 600 benchtop X-ray diffractometer (30 kV/10 mA at 0.05° increments from 3° to 70°) using the Rigaku PDXL software. Total carbonate content of bulk rock was measured using a digital calcimeter (Zammit et al., 2022). Semi-quantitative XRF major element abundances were measured on a total of 114 samples from the il-Blata section using an Olympus Delta Innov-X XRF gun (Zammit et al., 2022). From these samples a subset of 57 samples pertaining to depositional interval 2 was presented in this study. The ratios of iron, phosphorus and sulfur to the main components of the sediment (i.e., Fe/(Ca+Si+Al), P/(Ca+Si+Al), S/(Ca+Si+Al)) were considered. Relationships among these elemental ratios were used to roughly assess the oxygenation states of the sediment at the time of deposition since iron tends to be incorporated authigenically in anoxic sediments into sulfur-bearing phases (e.g gregite, mackinawite, pyrite) while iron-oxides (goethite, lepidocrocite) are major phosphorous sinks. Detailed methods and all bulk carbonate and elemental data are found in Zammit et al., (2022).

A total of five representative samples (MG-55, MG-57, MG-81, MG-91, MC-05) (Fig. 2) were analysed for both total inorganic carbon (TIC) and total organic carbon (TOC). TIC was determined using infra-red carbon and sulfur analyser Eltra CS500 (Eltra, Neuss, Germany) and carbonate CO_2 on a Coulomat 7012 Strohlein instrument. Decomposition temperature of 1350–1450°C with a sample weight of 50–200 mg for carbon concentrations ranging from 0.01–95.0%. The absorption of released CO_2 gas was measured in the infrared range. The TOC-measuring device was calibrated using an in-house reference material before initiating the analysis, and its operations settings were adjusted as per the manufacturer's guidelines. The determination has an accuracy of ±3% of the reported value.

The carbon and oxygen isotope ratios of carbonate phases were analysed following removal of organic carbon by hydrogen peroxide. The $\delta^{13}C$ and $\delta^{18}O$ values for calcite were obtained by first digesting the samples at room temperature with 100% phosphoric acid following McCrea (1950). To obtain the same stable isotope records for dolomite, the samples were decalcified by treatment with 10% HCl for 20 minutes, then thoroughly rinsed five times with deionized water. The residual fraction was subsequently digested at 100°C with 100% phosphoric acid. The CO_2 released from each phase was separately analysed for $\delta^{13}C$ and $\delta^{18}O$ values using a DELTA V mass spectrometer (Thermo Fisher Scientific), coupled with an EA-1108 elemental analyser (Fisons) and a ConFlo IV reference gas interface. Isotope ratios are reported in δ-notation (‰) relative to Vienna PeeDee Belemnite (VPDB) using the equation $\delta(\text{Sample}) = [(R_{sample}/R_{standard}) - 1] \times 10^3$, where R represents the $^{18}O/^{16}O$ or $^{13}C/^{11}C$ ratio. The acid fractionation factors used were 1.00908 for CO_2 derived from carbonates in the (Ca,Mg,Fe)(CO_3) system (Rosenbaum & Sheppard, 1986) and 1.01025 for calcite (Friedman & O'Neil, 1977). The in-house long-term reproducibility for $\delta^{13}C$ and $\delta^{18}O$ measurements (2σ confidence precision level), is based on combined measurement of IAEA NBS-18 and in-house standards (Carrara Marble), and it is better than ±0.1‰

Petrographic analysis

Based on initial field evaluation and geochemical analysis, four representative samples (MG-55, MG-91, MC-01, MC-06) from the Depositional Interval 2 (Zammit et al., 2022) of the il-Blata Section were selected (Fig. 2). Samples MG-55 (SP IV) and MG-91 (SP VI) were obtained from fine grained carbonate mudstone sequences while MC-01 (SP VII) and MC-06 (SP VII) are from cream coloured fine grained siliceous carbonate sequences rich in chert nodules (Zammit et al., 2022). Samples were selected in order to represent the evolving stratigraphy of the section. These samples underwent in-depth petrographical analysis supported by scanning electron microscopy coupled with energy dispersive spectrometry (EDS). A MIRA3 GMU scanning electron microscope (Tescan, Brno) combined with a Nordlys Nano (Oxford Instruments, Oxfordshire) energy dispersive X-ray spectroscope were used. Freshly broken and polished thick sections were used for the analysis.

Results

Lithology

The bedsets considered here are divided into four sedimentary packages (SPs) on basis of lithology (Zammit et al., 2022) (Fig. 2). SP IV consist of organic rich very thinly bedded calcareous marls containing ~60% carbonate (Fig. 3a), these beds are capped by SP V carbonates. SP V is composed of thin to medium bedded mudstone/wackestone facies. Within this package there are phosphatic pebble horizons embedded in the limestone containing small (~1 cm) pebbles of apparent allochtonous origin (Fig. 3b). This sedimentary package is similar to the underlying marine carbonates described in SP III of Depositional Interval 1 (Zammit et al., 2022). Its carbonate content is about 70% and signs of bioturbation are present. SP VI is similar to SP IV but is more finely laminated (Fig. 3c-d) with no signs of any bioturbation, the transition from SP V to SP VI is conformant (Fig. 3c). The finely laminated beds pertaining to SP VI alternate at the millimetric scale between very dark and lighter layers (Fig. 3d). The uppermost part of the bed sets considered here (SP VII) consist of siliceous limestones with large cherty nodules in distinct horizons (Fig. 3e-g). Its carbonate content is relatively low, ~30%, and the package overlies the dark layers of SP VI conformably with a swift colour change to creamy white marls (Fig. 3f) and the incidence of cherty nodules of various sizes (Fig. 3e-g).

Elemental, mineral and isotopic composition

Carbonate content tends to be generally high within SP IV to SP VI with values varying between 60 and 70 % by weight, although with a notably low (54%) occurring towards the base of the organic-rich SP VI. There is a trend towards low carbonate values within SP VI and a significant drop of total carbonate in the cherty SP VII (Fig. 4a). The elemental ratios of iron and phosphorous to the major elements in the section (calcium, silicon and aluminium) (Fe/(Ca+Si+Al), P/(Ca+Si+Al)) describe similar patterns throughout the studied interval and are generally similar to the ratio of S/(Ca+Si+Al). These ratios are generally high within SP V and SP VI, dropping significantly within the cherty SP VII (Fig. 4b-c).

TIC remained unchanging throughout most of the succession with values ranging between 8.0 and 9.0 % by weight. Peak values of around 9.0 % are within the dark SP VI carbonate mudstones , dipping to ~8.0 % in the cherty mudstones of SP VII. The trend remains the same as that of the carbonate content, as expected (Fig. 4d). The TOC content is generally high for marine carbonates throughout the section with the least value being 0.78%,

which occurs within the cherty SP VII. Highest TOC value of 1.37% is found near the top of SP VI (Fig. 4e) corresponding to the darker and most finely laminated parts of the section.

The semiquantitative EDS analysis reveals that Fe-carbonate in the cements never exceeds 25% by mass, suggesting a composition more consistent with dolomite or intermediate members of the dolomite–ankerite series, i.e., ferroan-dolomite, given that Ca remains at ~50% of the total cation content (Table S3 in the supplementary material). The contribution of Fe-dolomite component of the total carbonate tends to increase with height in the section, reaching a maximum of 20% within the organic rich SP IV beds and remaining high in the overlying cherty beds of SP VII (Fig. 4f). A similar trend had been observed in Maltese outcrops at il-Qammieħ and Xatt l-Aħmar, suggesting that this was a regional signal and not a localised one at il-Blata (John et al., 2003).

Stable isotopes ($\delta^{18}O$ and $\delta^{13}C$) in the calcite mineral phase of the studied samples tend to remain similar throughout the interval with very little variability (Fig. 4i). However, the same cannot be said about the $\delta^{18}O$ and $\delta^{13}C$ as measured for the Fe-dolomite component of the total carbonate (Fig. 4i). Both the $\delta^{18}O$ and $\delta^{13}C$ show considerable variation with $\delta^{13}C$ reaching a minimum of −1.24 ‰ within the organic-rich SP VI samples and then increasing significantly to 1.81 ‰ within the cherty interval of SP VII. The least value for $\delta^{18}O$ is 0 ‰ in SP V and maximum of 2.37 ‰ within SP VII. The $\delta^{18}O$ values increase by around 2 ‰ in the shift from the organic-rich SP VI to the silica-rich SP VII while the change in $\delta^{13}C$ for the same interval is around 3 ‰. In general, the lowest values of Fe-dolomite $\delta^{13}C$ have good correspondence with the lowest values in the bulk rock $\delta^{13}C$ record and coincide with lowest values in $\delta^{13}C$ of organic carbon and high TOC levels.

Petrographic analysis

In general, all samples display fine crystalline matrix-selective dolomitisation. Dolomite crystals are 4-20 μm in size, planar-e to planar-s, and are usually zoned. As per SEM-EDS analysis, dolomite is iron-rich (4.1 to 24.9 % by weight). The crystals within SP IV (sample MG 55) present zoning that consists of alternations of variably Ca- and Fe-rich bands (Fig. 5a). Calcitic foraminiferal tests are typically comprised of micrite and/or microspar matrix and are at times punctually phosphatized. Isopachous dogtooth fringes overlain by blocky calcite crystals are frequently observed in different parts of the section (SP VI, VII) (Fig. 5b,c,d). Silicification of planar-e rhombohedral crystals is commonly observed, but, interestingly, the process does not appear to have affected calcitic foraminiferal tests. Opal lepispheres were observed in SP VII (Fig. 5e). Putative prokaryote cells appear to be preserved in intra-chamber cements (SP IV) and at times, there are also spar and microspar aggregates presenting textures suggestive of precipitation in microbial exopolymers (Fig. 5f). These include mucilage strings and spheroidal features that are comprised of nanocrystalline carbonate (Bontognali et al., 2008).

Pyrite was observed in all samples, appearing as framboids with composite diameters ranging from ~3 to ~11 μm and comprised of individual crystallites in the nanometre scale (< 400 nm). Pyrite also occurs as (presumed) replacement of aragonitic pellets, but it is notably absent as single crystals. Framboidal pyrite can either occur in the matrix (SP VII) (Fig. 5 g, h) or as in SP IV, infilling the chambers of planktonic foraminifera (Fig. 5b). Microcrystalline fibrous gypsum can also be found infilling the chambers of foraminifera (MG 91 and MC 06), and this cement is often silicified (Fig. 5i). Gypsum cement was observed not only in the chambers of planktonic foraminifera species but also in large elongated benthic foraminifera present in SP VII (Fig. 5j).

Discussion

Indicators of stratification of the Central Mediterranean water column during an Early Miocene anoxic event

In all representative samples observed via SEM, framboids are present within planktic foraminiferal tests and also in the muddy matrix (Fig. 5b,g,h). Framboid sizes can be indicative of environment of deposition (Rickard, 2019). Our data from the il-Blata records demonstrates differences in mean framboid size between the organic rich section (SP VI) and the rest of the samples. In general mean framboid sizes are considered small, and never exceed 10 μm, suggestive of pyrite growth within an anoxic and sulfur rich water column (Wilkin et al., 1996). Pyrite tends to accumulate and grow into larger framboid sizes (10 μm up to 40 μm) once the particles settle on the seafloor and grow in iron sulfide supersaturated fluids (Wilkin et al., 1997). Such conditions are best achieved in settings characterized by Eh fluctuation where polysulfides intermediates can be cycled (Ohfuji & Rickard, 2005). The presence of small sized (<10 μm) framboids in foraminiferal tests suggests that these conditions may have developed in the water column (Rickard, 2019). Framboid sizes within the most organic rich (TOC ~ 1.4%), finely laminated SP VI layers tend to be generally larger than framboids within the rest of the section (Fig. 5g). This general increase in framboid diameter (mean ~ 7 μm) coupled with the very fine laminations and no clear indication of bioturbation (Fig. 3d) within this sedimentary package highlights a change in the sedimentary environment. Framboids with diameters in the region from 6 μm to 10 μm can be indicative of weakly

oxygenated bottom waters (lower dysoxic), as seen in finely laminated and non-bioturbated sediments (Wignall & Newton, 1998). This aligns with the sedimentary characteristics of SP VI at il-Blata. However, pyrite framboid formation could also occur during early burial in the sediment rather than in the water column. The lack of single crystals and the observed replacement textures suggest an excess of reactants (iron and polysulfides) in the system, which supports the potential for pyrite growth within the sediment under evolving redox (Bond & Wignall, 2010).

The presence of gypsum in SP VI (Fig. 5i) further highlights that change and coupled with high sulfur concentrations elevated Fe and P to major element ratios and a significant negative spike in bulk $\delta^{13}C$, coinciding with a negative excursion in both the Fe-dolomite and organic carbon $\delta^{13}C$, indicates early diagenesis under a ferruginous (high iron, low sulfide) setting that precludes significant sulfate reduction (Fig. 5 b,c,g,i). This also coincides with the layer containing a high proportion of Fe-dolomite (Fig. 5f). These reactions would occur very close to the seafloor within centuries or millennia in a way similar to what has been documented in the Eastern Mediterranean. In the Late Miocene (Messinian) to Pleistocene, organic-rich deep water sediment of the Eastern Mediterranean, sulfate reduction and formation of authigenic minerals occur within decimetres below the seafloor, as documented in the Integrated Ocean Drilling Program (IODP) and Deep Seas Drilling Project (DSDP) Leg 42A Sites 374 (Messina Abyssal Plain) and 376 (Florence Rise) (Sigl et al., 1978). Cores from these sites reveal sulfur-iron interactions such as dolomite cementation features that are at times accompanied by gypsum (Passier & De Lange, 1998). Importantly, for these processes to occur, the effects of organic matter reduction must be paired with a source of alkalinity to counteract pH changes during precipitation (Petrash et al., 2017; Rubin-Blum et al., 2014; Sela-Adler et al., 2015; Sisma-Ventura et al., 2022; Wurgaft et al., 2019). This alkalinity might be sourced from riverine base cation and soil-derived nutrient inputs or from the dissolution of carbonate in the sediment. We discuss additional influence of riverine input on the sedimentary deposits at il-Blata below.

Excess Fe^{2+} incorporated into dolomite and, to a minor extent, framboidal pyrite could be supplied by two main sources: (1) atmospheric deposition and (2) fluvial fluxes. However, in an oligotrophic configuration, exclusive fertilisation by dust would not be sufficient (Herut et al., 2002) and upwelling systems are, for the most part, iron-limited (Frost & Franzen, 1992; Hutchins et al., 2002). Therefore, in order to achieve excess nutrients conducive to oxygen-depletion and have an iron excess in the environment a fluvial input has to be considered. In this scenario, the presence of Fe-dolomite and the preservation of carbonates in the il-Blata section supports models of enhanced continental runoff onto the Central Mediterranean during the Early Miocene, in a similar way to that observed in the Miocene Monterey Formation (Baker & Burns, 1985). The terrigenous fluxes delivered ferric iron while decomposing organic matter produced the necessary reducing conditions that allocate solubilisation of reducible iron in the pore waters, followed by its incorporation into dolomite. These terrigenous inputs also altered pore water biogeochemistry, increasing microbial activity and promoting pore water dolomite saturation via alkalinity generation.

Alternative dolomitisation models do not appear to be applicable here. The burial depth, local thermal gradient and lack of evidence for thermogenic fluid migration precludes thermogenic dolomitisation. Additionally, the paleogeography and depositional water depth do not support the conditions necessary for mixing zone dolomitisation (Bellanca et al., 2002; Dart et al., 1993). While the presence of gypsum might, under a coastal depositional scenario suggest a reflux dolomitisation path, the absence of any known lagoonal facies in the Pelagian Islands during this period challenges this model (Pedley et al., 1978; Pedley, 1996). Therefore, in the depositional context of the Globigerina Limestone Formation, gypsum is more likely to be a by-product of sedimentary sulfur cycling occurring beneath a density- and redox-stratified water column (Petrash et al., 2022). In line with our fluvial input interpretation, gypsum can be attributed to a stage of increased bottom currents that caused submarine erosion and facilitated the inflow of ferric iron-bearing particles into anoxic bottom waters overlying organic-rich seafloor sediments. The presence of Fe-dolomite and to a lesser extent pyrite, strongly indicates significant iron reduction and redox gradients, emphasizing the importance of early diagenetic iron reduction in organic-rich sediments. Burial diagenesis then further enhanced the utility of any early-formed dolomite precursors as valuable proxies for reconstructing paleoenvironmental conditions (Bathurst, 1987; Bottrell & Raiswell, 1989) leading to the strata-bound abundance of dolomite that we observed in the il-Blata section.

The decoupling between the bulk stable isotope records $\delta^{18}O$ and $\delta^{13}C$ within SP VI (18.90 Ma to 18.76 Ma) and deviation of these values from the global benthic records (Fig. 4g and 6a) can now be discussed. The reason for this decoupling can be attributed to a changing depositional environment and its effects on early diagenesis, the establishment of redox zonation within the water column and mineral specific stable isotope composition (Blanchet et al., 2021). Fe-dolomite at the il-Blata section exhibits $\delta^{13}C$ values (Fig. 4i) that are less negative than those of dissolved inorganic carbon (DIC) from iron-reducing environments (Curtis et al., 1986), which suggests mixed carbonate ion source. This isotopic signature likely results from the partial contribution of DIC from Early Miocene seawater and ^{13}C-depleted carbon from organic matter oxidation under iron-reducing

conditions. Substitution of Mg^{2+} (and Ca^{2+}) by Fe^{2+} in dolomite lattices indicates ferruginous, anoxic pore waters, where Fe^{2+} ions can accumulate and be incorporated into the dolomite lattice (Barnaby & Rimstidt, 1989; Clarkson et al., 2014). Iron is incorporated into the carbonate crystal lattice when it occurs in the ferrous (Fe^{2+}) ionic state, and this is controlled by the reducing pore waters. Pore waters poor in oxygen can facilitate the accumulation of Fe^{2+} ions which can be incorporated into diagenetic carbonates. The conditions facilitating Fe^{2+} and Mg^{2+} co-precipitation with Ca^{2+} into dolomite were likely driven by chemolitotrophic respiration sustaining alkalinity production and proton consumption in the pore waters during growth (Petrash et al., 2017, 2021).

Notably, the peak formation of Fe-dolomite in SP VI is associated with a negative $\delta^{13}C$ excursion in the bulk record (Fig. 4f, g), indicating that these stratigraphic levels likely formed during the peak of ferric iron reduction and during shallow burial. This likely occurred in the absence of substantial concentrations of sulfide as a byproduct of microbial sulfate reduction, which would have otherwise titrated iron out from the pore waters as pyrite and prevented substantial co-precipitation with Mg and Ca in carbonate phases observed across the studied section (Berner, 1984; Poulton & Canfield, 2005; Raiswell & Canfield, 1998). However, in the absence of iron, organic matter can absorb the excess sulphur through a "vulcanisation" process rendering it inaccessible for microbial respiration (Aizenshtat et al., 1995; Sinninghe Damst'e et al., 1989; Urban et al., 1999).

A subsequent shift towards positive $\delta^{13}C$ values in the Fe-dolomite component is observed in the upper sedimentary packages (Fig. 4g). This points to a shift in the fluid-buffered diagenetic environment were iron-dolomite formed. In shallow to intermediate burial realm, open diagenetic systems are fluid-buffered, with isotope exchange dominated by pore fluid flow through partially lithified carbonate sediments (fluid-controlled) (Bjørlykke & Jahren, 2012; Higgins et al., 2018). Such a shift possibly coincided with changing basin redox stratification conditions, or were the result of changing contribution of seawater vs. formation waters in the precipitation milieu, previously poised to high carbonate precipitation rates (Immenhauser, 2022). Additionally, the presence of significant chert in these layers, coupled with a decrease in Fe/major element ratios (Fig. 4b) in the bulk sediment record is also indicative of changes in the oxidation and mineral saturation state of the sediments (Clarkson et al., 2014).

Changes in nannofossil assemblages can also be an indicator of enhanced land surface run-off leading to the establishment of eutrophic surface waters (Auer et al., 2014). In this regard, the increased presence of *H. Carteri* in the studied section (Baldassini & Di Stefano, 2015) may be indicative of eutrophic surface conditions and a strong input of terrigenous material (Auer et al., 2014; Oretade, 2021). However, other taxons indicative of these conditions have not been reported and, coupled with the fact that this taxon remains high throughout the section may preclude its validity as a useful indicator. This argument in itself does not present a fully quantitative and systematic palaeoecological study that is needed to properly make these claims. In the absence of such, the available data offers only limited constrains on the trophic conditions in the region.

Significant amounts of silica in the upper layers (SP VII) coupled with a decrease Fe/(major element) in the bulk record are suggestive of a change in the oxidation and saturation state of the basin that was recorded in the sediment (Fig. 4b). The clay-rich nature of the underlaying SPVI may have prevented silicification of underlying sediment by offering a barrier to the overlying fluids. The silica concentrates in chert nodules seen in specific horizontal layers in an almost periodic pattern. This may suggest that the processes leading to their formation is associated with cyclical blooms of siliceous organisms in surface waters impacted by Fe 'fertilisation' (Li et al., 2022). Oxidation of organic matter within carbonate-rich sediments is considered as a possible mechanism for nodular chert formation at sites where 'carbonate ghosts' are replaced by chert nodules (Fig. 3g) (Maliva & Siever, 1989). In addition, a shallow burial silicification mechanism of carbonate was likely driven by an alkaline, i.e. silica-oversaturated fluid, permeating the bottom stratified column and by diffusion in the upper sediments. There the fluid lead to partial replacement of early formed dolomite cements (Petrash et al., 2016, and references therein). This silica-rich fluid would have induced the development of a coupled dissolution-precipitation reaction front, leading to the pseudomorphic replacement of metastable Ca-rich precursors to dolomite. However, already stabilized (to calcite) micritic fabrics of foraminifera as well as the more stable pre-existing early diagenetic/primary (Mg-rich) dolomite (see Meister et al., 2022) were not silicified. The replacement of metastable early diagenetic carbonates by silica is believed to have occurred under shallow burial diagenetic conditions and under the influence of diagenetically evolved seawater. The pore waters would have then possibly been saturated with regard to gypsum, as evidenced by the presence of pseudomorphic gypsum partially silicified within benthic foraminifera chambers (Fig. 5 i,j). Density stratification in isolated basin settings is conducive to the diagenetic process evaluated here, and it is also responsible for the establishment of bottom water anoxia (Meyer & Kump, 2008).

The TOC measured in this study (Fig. 4e) is generally high for marine carbonates and is highest in the dark green, finely laminated mudstones pertaining to SP VI exhibiting a maximum value of 1.37%. The definition originally proposed by Kidd et al., (1978), considers pelagic mudrocks containing between 0.5 % to 2 % by weight

to be 'sapropelic' and distinct pelagic layers thicker than 1 cm containing over 2 % TOC to be true 'sapropels'. Using this definition the layers investigated here are defined as 'sapropelic'. Their dark and finely laminated nature also defining them as such (Cramp & O'Sullivan, 1999). This makes the il-Blata organic-rich layers very important in being sapropelic deposits from relatively shallow pelagic environments at a time when no such deposits were widespread in the Mediterranean. This further highlights the importance of land-based sections in our understanding of climatic evolution and justifies the search for further land or deep-sea sections that can offer insights into climatic evolution during the Early Miocene. In particular, regional and global climate dynamics during the Burdigalian and poorly known. The initial closure of the Mesopotamian Seaway (Bialik et al., 2019) at the time, cessation of low latitude phosphatisation (Föllmi et al., 2008; Zammit et al., 2022) and a global shark extinction event suggest that this time period merits further investigation (Sibert & Rubin, 2021). It is encouraging to note similarities in lithostratigraphy and minerology with other sites outcropping in the Maltese Islands (John et al., 2003), Sicily (Föllmi et al., 2008), Central Italy (Auer et al.,2015., 2016; Brandano et al., 2016; Cornacchia et al., 1996) and North Africa (Essid et al., 2019; Riahi et al., 2015), yet due to numerous hiatuses and at times limited age constraints of the sections, a precise stratigraphic correlation between these sites remains problematic. This makes the il-Blata section an important site in understanding the evolution of the Mediterranean basin and its unique tectono-climate characteristics and highlights the need for further detailed investigation of the il-Blata site and stratigraphic correlation between il-Blata and other contemporaneous outcrops in the region.

Climatically controlled Central Mediterranean sedimentary processes

The Maltese depositional environment underwent a dramatic change following MSR-1 (20.35 Ma to 19.05 Ma), with the shift from low sedimentation rate phosphorite bearing marine limestones to high sedimentation rate continentally influenced mudstones (Zammit et al., 2022). A drop in carbonate content observed within the studied interval is correlatable with the influx of continental material via riverine systems that were activated at the time and flooded the low productivity marine system. Our new records allow us to further understand the climatic history of the central Mediterranean in finer detail. As previously proposed (Bialik et al., 2019; Zammit et al., 2022), the tectonic and eustatically forced decrease in surface water flow through the Mesopotamian Seaway would have had a direct effect on North African hydroclimate by favouring intensification of Atlantic circulation.

As the newly enclosed Mediterranean basin became more sensitive to modified circulation effects, the seasonality of monsoonal activity, which is strongly modified by eccentricity (Wu et al., 2021), enhanced the delivery of terrigenous material sourced from North Africa. This created paleoproductivity plumes in surface Mediterranean waters that had transient excess of bio-limiting nutrients, such as iron and silica. An estimate of the extension and areal sensibility of these Early Miocene plumes to minor fluxes change can be provided by considering the extension of Nile plumes prior to the construction of the Aswan High Dam in Egypt. Then, the Nile plume extended as far north as Beirut during peak activity (Oren, 1969). Considering that Beirut is over 400 km from the edge of the Nile Delta, it is reasonable to assume a similar range as the minimum extension. It is also likely that the extent of these plumes was larger during the peak fluxes associated with sapropelic events. Therefore, it can be assumed that any active fluvial systems in Libya and Tunisia (e.g. Fezzan and Chott systems; Fig. 1)) may have had plumes extending well into the area of the Maltese Islands during peak activity (Fig. 7a). In a Mediterranean flow system conditioned by a closed eastern gateway, surface waters entering from the Atlantic moved eastward and would have carried the Chott plume from the Gulf of Gabes into the Central Mediterranean (Fig. 7a). This would make the Chott system a more likely source of inorganic material over Malta than the Fezzan system that outflows from the Gulf of Sirte, since surface flow would have carried a plume from Sirte away from Malta.

Within the context of orbital forcing, high seasonality would result from times when the Earth's tilt, precession, and eccentricity produce significant seasonal contrasts. During these periods, the difference between summer and winter temperatures is heightened. This increased seasonality causes surface waters to warm significantly in the summer, creating a strong thermocline, a steep temperature gradient between the warm surface waters and the cooler, deeper waters. This thermocline acts as a barrier to vertical mixing, leading to a highly stratified water column (Grant et al., 2016). As a result, the deep waters can become anoxic (depleted of oxygen) because the oxygen consumed by biological processes is not replenished by mixing with the oxygen-rich surface waters. We propose that an enhanced supply of terrigenous material from Gabes drove up productivity and led to the establishment of poor oxygen conditions in the water column. The introduction of low-oxygen intermediate waters from the Aegean region is also possible in this closed eastern gateway configuration (Zirks et al., 2019) (Fig. 7a). This flux of oxygen-poor intermediate waters from the Aegean can also facilitate the formation of oxygen minimum zones.

Within the limitations of the data, it is possible to present a hypothesis that the peak of Fe-dolomite generation, peak TOC, and negative $\delta^{13}C$ excursion coincided with a time of maximum eccentricity (400 ky cycle)

and greatest peak-to-peak fluctuations in the precession cycle (Fig. 6). However, since the site has not yet been astronomically tuned, this hypothesis needs to be evaluated with caution and the following inferences are only of a suggestive nature. The Fe-dolomite formation can be attributed to early diagenesis influenced by a combination of an enclosed Mediterranean, generating the necessary ocean current systems and the right conditions for intermediate low oxygen waters forming in the Aegean region, and astronomically modulated by a ~400 kyr cycle. It would be instructive to resample the il-Blata section at very high-resolution and test this hypothesis to confirm or deny the influence of astronomical forcing factors on the depositional and diagenetic trends observed. The fact that anoxic sediments in the Mediterranean can be modulated by a ~400 kyr cycle has previously been reported for Middle Miocene phosphorite bearing carbonate deposition in Central Italy (Auer et al., 2016).

Redox-controlled siliceous productivity bloom

Iron-bound phosphorus can be incorporated as phosphates in sediments featuring euxinic (i.e., high sulfide anoxic conditions) conditions (Dijkstra et al., 2014). The data presented here indicates an association between iron and phosphorus, although such data needs to be considered with caution since XRF records are semi-quantitative and no extraction procedures were used for the measurement of phosphorus. Still, there is general correspondence between the Fe and the P records. The amounts of P and Fe trapped in sediment changes swiftly with the lithological change to cherty limestones and the rapid shift of the Fe-dolomite stable isotope records (Fig. 4b, i). Both iron and phosphorous can be re-released into pore waters when the oxygenation state changes (Filippelli et al., 2003).

It is likely that following the peak in hydrological activity over North Africa at 18.82 Ma, the diminishing of the nutrient flux into the central Mediterranean and possible eustatic mediated (Miller et al., 2020) re-opening of the Mesopotamian gateway allowed for the return of a mixed and oxygenated water column (Fig. 6c and 7b). Such a system would have favoured the remobilisation of Fe and P back into the water column; while upwelling systems could have aided the return of these biolimiting nutrients to the surface. A silica phytoplankton bloom would have ensued, which can account for increased silica saturation in the sediment. Evidence for a bloom in siliceous organisms can also be attained by noting a peak in the abundance of the zeolite mineral clinoptilolite recorded in the Middle Globigerina Limestone member (John et al., 2003). Although, John et. al. (2003) attribute this peak in clinoptilolite to a volcanic input, the presence of siliceous deposits at il-Blata and the lack of evidence for regional volcanism during the Early Miocene would more likely suggest that the zeolite is indicative of a siliceous bioproductivity bloom (Karpoff et al., 2007). This is further supported by records from North Africa that show that the siliceous deposits associated with the Early Miocene Numidian Formation are of biogenic and not volcanic origin (Ben Yahia et al., 2019; Essid et al., 2019). As biogenic silica fell to the seafloor, the newly available oxygenated state would have decomposed organic matter in the carbonate matrix creating condition for silicification in spaces vacated by 'ghosts' of carbonate precursors (Fig. 3g, 7b) (Maliva & Siever, 1989).

The change from a foraminifera dominated to a siliceous plankton dominated surface environment might be attributed to a number of factors. Possible general global warming conditions at the time (Westerhold et al., 2020), coupled with high dissolved inorganic carbon may have inhibited planktonic foraminifera as evidenced by poor preservation and generally small sized planktonic forms. The availability of silica from continental sources coupled with the release of iron and phosphorus from the sediment could have allowed for a short-lived (18.76 Ma – 18.62 Ma) bloom in siliceous organisms during a time of low seasonality. The central Mediterranean shifts again to a foraminifera dominated (Mourik et al., 2011) and phosphorite bearing (Föllmi et al., 2008) marine system following this episode in conjunction with the global shift in climate associated with the Monterey excursion (Jacobs et al., 1996). The global Monterey excursion would have led to high sea-levels triggering the intermittent reopening of the Mesopotamian Seaway and influencing upwelling systems in the region up till the permanent closure of the Mesopotamian Seaway (MSR-2) during the Middle Miocene expansion of the Antarctic ice sheet (~14 Ma).

Early Miocene organic-rich facies in the Central Mediterranean. The oldest Mediterranean sapropelic deposits?

Present day circulation in the Mediterranean is driven by density changes whereby warm and fresh Atlantic surface waters ($S \approx 36$ PSI, $T \approx 16$ °C) (Béranger et al., 2005), entering from the Strait of Gibraltar, are transformed into salty and cool intermediate waters via intense evaporation in the northern parts of mostly the eastern parts of the basin (Brenner, 2012). This intense halothermal circulation and the enclosed nature of the basin is conducive to the formation of well-oxidised surface waters reaching the seafloor resulting in a well oxygenated water column (Rohling et al., 2015). However, this configuration was not a constant feature of the region through its geological history.

Periodic episodes of oxygen starvation in Mediterranean bottom waters have been recorded in the Mediterranean basin since the Early to Middle Miocene (Athanasiou et al., 2021; Bialik et al., 2022; Rohling et al., 2015; Taylforth et al., 2014). These are associated with periods of high seasonality in orbital parameters (maximum eccentricity) (Mancini et al., 2023). Evidence of these episodes comes from the deposition of sapropels, which can serve as an indication of shifts in the general mode of circulation.

During the Pleistocene, these perturbations in the general circulation and stratification of the water column were driven by surges in freshwater inputs such as those from the Nile during times associated with high northern summer insolation (Grant et al., 2016). It has been generally considered that inputs of low-density fresh waters can generate a highly stratified water column, which coupled with high fluxes of dissolved inorganic carbon in surface waters can lead to high utilisation of oxygen in surface layers and the eventual depletion of oxygen further down the water column and the formation of oxygen minimum zones (Blanchet et al., 2021). It has been recently suggested that a key component in the formation of sapropels in the Eastern Mediterranean is the formation of an intermediate water mass that is depleted in oxygen but is neither anoxic nor euxinic (Zirks et al., 2019). It has been shown that during the Holocene (~8.2 ka) such a water mass formed in the Aegean and migrated both east and west reaching the Levantine Basin in the SE and the Adriatic basin towards the west. The oxygen dissolved in this water mass progressively decreased as these intermediate waters moved towards the Nile delta plume and encountered sinking dissolved inorganic matter (Zirks et al., 2019). Therefore, Mediterranean sapropel formation can be seen as being driven by the formation of an intermediate water-mass poor in oxygen in combination with a strong seasonal component affecting Nile discharge. Such an intermediate water mass would be formed due to climatic reasons associated with global cooling driving enhanced convection in the enclosed Aegean region (Filippidi et al., 2016; Filippidi & Lange, 2019).

The transition to an enclosed configuration in the Miocene would favour the formation of these organic-rich layers. Geological evidence for the existence of early Mediterranean sapropels supports this interpretation. Unambiguous sapropelic layers first appear (13.5 Ma) following the final closure of the Eastern Mediterranean seaway (MSR-2 at ~14 Ma) (Grant et al., 2016) and it seems reasonable to assume that only an enclosed basin favours a circulation pattern conducive to periodic bottom water anoxia. There is also evidence for older 'proto-sapropelic' organic rich layers from field outcrops in Cyprus dated ~15.5 Ma (Athanasiou et al., 2021; Bialik et al., 2022). It is now known that the Eastern Gateway had already been severely restricted during the Early Miocene (MSR-1) (Bialik et al., 2019; Zammit et al., 2022) raising the possibility of water column stagnation during times of low east to west oceanic surface water flows. There is also the possibility that this gateway was intermittently re-opened during the Miocene Climatic Optimum, ~17 Ma (Cornacchia et al., 2021) via a eustatic control, and that an enclosed basin configuration existed for a geologically short-lived interval between MSR-1 (~20 Ma) and the Miocene Climatic Optimum (~17 Ma).

It has recently been proposed that the shift from predominantly marine limestones bearing phosphatic hardgrounds to clay/mud rich facies pertaining to the Middle Globigerina Limestone formation in Malta was the result of a shifting climate over western North Africa (Zammit et al., 2022). This shift towards a wetter climate has been considered to be a land-atmosphere-ocean response to gateway changes causing an intensification of Atlantic circulation and the ensuing climatic influence on the North African landmass (Zammit et al., 2022). The il-Blata facies of depositional interval 2 investigated in this study were deposited during this short period in which Mediterranean surface water flow from the east was severely reduced, and the long-standing east to west surface flow was switched to a west-east flow sinking in the east in a thermohaline conveyor system. Coupling the increased runoff from North Africa with the new circulation system and the possibilities of formation of de-oxygenated intermediate waters (in the northern basins of the Eastern Mediterranean), it is very likely that anoxic (ferruginous, as per formation of iron) and/or transiently euxinic conditions formed in the pelagic/hemi-pelagic zones of Central Mediterranean and influenced subsurface stabilisation of Fe-dolomite in the sediments of the il-Blata section. The presence of planktonic foraminifera infilled by gypsum may indicate that density saturation was established in the water column at the time of deposition These gypsum-saturated waters may as well have been established in the sediment-water interface, thus leading to pore-water oversaturation with regard to gypsum, with the mineral accumulating in the chambers of benthic foraminifera. Those density and redox stratified conditions favoured accumulation of organic matter, with TOC measured in this study being generally high for marine carbonates, and with a maximum value of 1.37% in SP VI indicating that sapropelic layers formed within this sedimentary package. The possible re-opening of the Mesopotamian Seaway precluded the low oxygen conditions and increased ventilation throughout the water column. A combination of available oxygen and nutrients led to a short-lived siliceous plankton bloom evidenced in the chert nodules of SP VII. Further examination of the gypsum infilling discrete foraminifera chambers using stable $\delta^{18}O$ and $\delta^{34}S$ would provide further insight, but this would require using high resolution in situ analyses such as NanoSIMS.

Conclusion

The formation of iron-dolomite, sapropelic layers, and chert in the outcrops of the Middle Globigerina Limestone member in Malta was a combination of interrelated factors. Foremost among these was the proximity of the Maltese Islands to now-extinct North African fluvial systems, particularly on the western side of the continent. These systems delivered freshwater, nutrients, and iron to surface waters, promoting a stratified water column and oxygen-depleted bottom waters featuring transient ferruginous states. The deltaic systems of the Gulf of Gabes likely played a significant role as primary sources of iron into the marine realm, facilitating the formation of Fe-dolomite at sites like il-Blata in Malta.

During peak activity of these fluvial systems, surface waters in the Central Mediterranean became highly stratified, with limited oxygen availability. Organic matter decomposition under these conditions generated alkalinity and the establishment of reducing environments below the sediment-water interface, facilitating the solubilisation of ferrous iron into pore waters oversaturated with regard to carbonate. This ferrous iron, along with magnesium and calcium, was incorporated into early nucleated dolomite lattices under conditions of subsurface chemolithotrophic respiration, which promoted carbonate growth. The peak of these conditions, around 18.82 Ma, coincided with preserved sapropelic layers, marked by elevated TOC and negative $\delta^{13}C$ excursions. These layers highlight ferric iron reduction processes, where iron availability exceeded byproduct sulfide, precluding the formation of extensive pyrite and instead favouring Fe-dolomite precipitation. Burial diagenesis further enhanced these dolomite precursors, stabilizing them as paleoenvironmental proxies for reconstructing Early Miocene redox and depositional conditions.

Subsequent changes in global sea level reopened the Mesopotamian Seaway, altering Mediterranean water dynamics. This, combined with climatic changes, re-oxygenated the water column, suppressing conditions favourable for Fe-dolomite formation. Instead, re-oxygenation facilitated siliceous productivity blooms, with the oxidation of organic matter and deposition of silica leading to the formation of chert nodules. These nodules, preserved in SP VII, provide further evidence of the dynamic interplay of diagenetic and depositional processes during this interval. This study underscores the importance of the Mediterranean basin as a natural laboratory for investigating the interconnection between climatic and tectonic controls on sedimentary and diagenetic systems. The detailed records from Malta provide valuable insights into Early Miocene environmental dynamics and diagenetic pathways, particularly the role of fluvial inputs, redox stratification, and microbial processes in dolomite formation.

Acknowledgements

Acknowledgements are due to the Superintendence for cultural Heritage Malta for permission to collect samples from the il-Blata section (Permit SCH213/16). Paul Pearson is thanked for useful discussions. We are extremely grateful to Cedric John for constructive criticism and to the anonymous reviewer for useful feedback which has greatly improved this paper from its original form. Daniel Petrash acknowledges support of CGS (internal project TBD) during analytical data acquisition. Or M. Bialik is partially supported by the German (GEOMAR)—Israeli (University of Haifa) Helmholtz International Laboratory EMS-FORE. This is Cardiff EARTH CRediT Contribution 35.

References

Aizenshtat, Z., Krein, E. B., Vairavamurthy, M. A., & Goldstein, T. P. (1995). Role of Sulfur in the Transformations of Sedimentary Organic Matter: A Mechanistic Overview. 16–37. https://doi.org/10.1021/BK-1995-0612.CH002

Anastasakis, G. C., & Stanley, D. J. (1984). Sapropels and organic-rich variants in the Mediterranean: Sequence development and classification. Geological Society Special Publication, 15, 497–510. https://doi.org/10.1144/GSL.SP.1984.015.01.32

Athanasiou, M., Triantaphyllou, M. V., Dimiza, M. D., Gogou, A., Panagiotopoulos, I., Arabas, A., Skampa, E., Kouli, K., Hatzaki, M., & Tsiolakis, E. (2021). Reconstruction of oceanographic and environmental conditions in the eastern Mediterranean (Kottafi Hill section, Cyprus Island) during the middle Miocene Climate Transition. Revue de Micropaléontologie, 70, 100480. https://doi.org/10.1016/J.REVMIC.2020.100480

Auer, G., Piller, W. E., & Harzhauser, M. (2014). High-resolution calcareous nannoplankton palaeoecology as a proxy for small-scale environmental changes in the Early Miocene. Marine Micropaleontology, 111, 53–65. https://doi.org/10.1016/J.MARMICRO.2014.06.005

Auer, G., Piller, W. E., Reuter, M., & Harzhauser, M. (2015). Correlating carbon and oxygen isotope events in early to middle Miocene shallow marine carbonates in the Mediterranean region using orbitally tuned chemostratigraphy and lithostratigraphy. https://doi.org/10.1002/2014PA002716

Auer, G., Hauzenberger, C. A., Reuter, M., & Piller, W. E. (2016). Orbitally paced phosphogenesis in Mediterranean shallow marine carbonates during the middle Miocene Monterey event. Geochemistry, Geophysics, Geosystems, 17(4), 1492–1510. https://doi.org/10.1002/2016GC006299

Baker, P. A., & Burns, S. J. (1985). Occurrence and Formation of Dolomite in Organic-Rich Continental Margin Sediments. AAPG Bulletin, 69(11), 1917–1930. https://doi.org/10.1306/94885570-1704-11D7-8645000102C1865D

Baldassini, N., & Di Stefano, A. (2015). New insights on the Oligo-Miocene succession bearing phosphatic layers of the Maltese Archipelago. Italian Journal of Geoscience, 134(2). http://italianjgeo.geoscienceworld.org/content/134/2/355

Barnaby, R. J., & Rimstidt, J. D. (1989). Redox conditions of calcite cementation interpreted from Mn and Fe contents of authigenic calcites. Geological Society of America Bulletin, 101(6), 795–804. https://doi.org/10.1130/0016-7606(1989)101<0795:RCOCCI>2.3.CO;2

Barron, E. J., & Peterson, W. H. (1989). Model Simulation of the Cretaceous Ocean Circulation. New Series, 244(4905), 684–686.

Bathurst, R. G. C. (1987). Diagenetically enhanced bedding in argillaceous platform limestones: stratified cementation and selective compaction. Sedimentology, 34(5), 749–778. https://doi.org/10.1111/J.1365-3091.1987.TB00801.X

Bellanca, A., Sgarrella, F., Neri, R., Russo, B., Sprovieri, M., Bonaduce, G., & Rocca, D. (2002). Evolution of the Mediterranean basin during the Late Langhian - Early Serravallian: An integrated paleoceanographic approach. Rivista Italiana Di Paleontologia e Stratigrafia, 108(2), 223–239. https://doi.org/10.13130/2039-4942/5472

Ben Yahia, N., Sebei, A., Harris, C., Boussen, S., & Chaabani, F. (2019). Mineralogical and geochemical criteria to identify the origin and the depositional environment of the upper Numidian babouchite siliceous rocks, northwestern Tunisia. Journal of African Earth Sciences, 149, 487–502. https://doi.org/10.1016/j.jafrearsci.2018.09.010

Béranger, K., Mortier, L., & Crépon, M. (2005). Seasonal variability of water transport through the Straits of Gibraltar, Sicily and Corsica, derived from a high-resolution model of the Mediterranean circulation. Progress in Oceanography, 66(2–4), 341–364.

Berner, R. A. (1984). Sedimentary pyrite formation: An update. Geochimica et Cosmochimica Acta, 48(4), 605–615. https://doi.org/10.1016/0016-7037(84)90089-9

Bialik, O. M., Frank, M., Betzler, C., Zammit, R., & Waldmann, N. D. (2019). Two-step closure of the Miocene Indian Ocean Gateway to the Mediterranean. Scientific Reports, 9(1), 8842. https://doi.org/10.1038/s41598-019-45308-7

Bialik, O. M., Reolid, J., Kulhanek, D. K., Hincke, C., Waldmann, N. D., & Betzler, C. (2022). Sedimentary response to current and nutrient regime rearrangement in the Eastern Mediterranean during the early to middle Miocene (Southwestern Cyprus). Palaeogeography, Palaeoclimatology, Palaeoecology, 588, 110819. https://doi.org/10.1016/J.PALAEO.2021.110819

Bjørlykke, K., & Jahren, J. (2012). Open or closed geochemical systems during diagenesis in sedimentary basins: Constraints on mass transfer during diagenesis and the prediction of porosity in sandstone and carbonate reservoirs. AAPG Bulletin, 96(12), 2193–2214. https://doi.org/10.1306/04301211139

Blanchet, C. L., Tjallingii, R., Schleicher, A. M., Schouten, S., Frank, M., & Brauer, A. (2021). Deoxygenation dynamics on the western Nile deep-sea fan during sapropel S1 from seasonal to millennial timescales. Climate of the Past, 17(3), 1025–1050. https://doi.org/10.5194/CP-17-1025-2021

Bond, D. P. G., & Wignall, P. B. (2010). Pyrite framboid study of marine Permian–Triassic boundary sections: A complex anoxic event and its relationship to contemporaneous mass extinction. GSA Bulletin, 122(7–8), 1265–1279. https://doi.org/10.1130/B30042.1

Bontognali, T. R. R., Vasconcelos, C., Warthmann, R. J., Dupraz, C., Bernasconi, S. M., & McKenzie, J. A. (2008). Microbes produce nanobacteria-like structures, avoiding cell entombment. Geology, 36(8), 663–666. https://doi.org/10.1130/G24755A.1

Böttcher, M. E., & Dietzel, M. (2011). Metal-ion partitioning during low-temperature precipitation and dissolution of anhydrous carbonates and sulphates. European Mineralogical Union Notes in Mineralogy, 10(1), 139–187. https://doi.org/10.1180/EMU-NOTES.10.4

Bottrell, S., & Raiswell, R. (1989). Primary versus diagenetic origin of Blue Lias rhythms (Dorset, UK): evidence from sulphur geochemistry. Terra Nova, 1(5), 451–456. https://doi.org/10.1111/J.1365-3121.1989.TB00409.X

Boyd, P. W., & Ellwood, M. J. (2010). The biogeochemical cycle of iron in the ocean. Nature Geoscience, 3(10), 675–682. https://doi.org/10.1038/NGEO964

Bradbury, H. J., Vandeginste, V., & John, C. M. (2015). Diagenesis of phosphatic hardgrounds in the Monterey Formation: A perspective from bulk and clumped isotope geochemistry. Geological Society of America Bulletin, 127(9–10), 1453–1463. https://doi.org/10.1130/B31160.1

Brandano, M., Cornacchia, I., Raffi, I., Tomassetti, L., & Jones, B. (2016). The Oligocene–Miocene stratigraphic evolution of the Majella carbonate platform (Central Apennines, Italy). https://doi.org/10.1016/j.sedgeo.2015.12.002

Brenner, S. (2012). Circulation in the Mediterranean Sea. Life in the Mediterranean Sea: A Look at Habitat Changes, 5, 99–125. https://doi.org/10.1007/B107143/COVER

Bridges, T.F., Green, D.I., Ince, F. (2014). Ankerite: Its composition and formulae, and its status in the Northern Pennine Orefield. Journal of the Russell Society. 17 , 51-56:

Burns, S. J., & Baker, P. A. (1987). A geochemical study of dolomite in the Monterey Formation, California. Journal of Sedimentary Research, 57(1), 128–139. https://doi.org/10.1306/212F8AC6-2B24-11D7-8648000102C1865D

Casanova-Arenillas, S., Rodríguez-Tovar, F. J., & Martínez-Ruiz, F. (2022). Ichnological evidence for bottom water oxygenation during organic rich layer deposition in the westernmost Mediterranean over the Last Glacial Cycle. Marine Geology, 443, 106673. https://doi.org/10.1016/J.MARGEO.2021.106673

Cipollari, P., & Cosentino, D. (1995). Miocene unconformities in the Central Apennines: geodynamic significance and sedimentary basin evolution. Tectonophysics, 252(1–4), 375–389. https://doi.org/10.1016/0040-1951(95)00088-7

Clarkson, M. O., Poulton, S. W., Guilbaud, R., & Wood, R. A. (2014). Assessing the utility of Fe/Al and Fe-speciation to record water column redox conditions in carbonate-rich sediments. Chemical Geology, 382, 111–122. https://doi.org/10.1016/j.chemgeo.2014.05.031

Cornacchia, I., Brandano, M., & Agostini, S. (2021). Miocene paleoceanographic evolution of the Mediterranean area and carbonate production changes: A review. Earth-Science Reviews, 103785. https://doi.org/10.1016/J.EARSCIREV.2021.103785

Cornacchia, I., Brandano, M., Agostini, S., & Munnecke, A. (1996). Neodymium isotopes of central Mediterranean phosphatic hardgrounds reveal Miocene paleoceanography. 2015. https://doi.org/10.1130/G50118.1

Cramp, A., & O'Sullivan, G. (1999). Neogene sapropels in the Mediterranean: a review. Marine Geology, 153(1–4), 11–28. https://doi.org/10.1016/S0025-3227(98)00092-9

Curtis, C. D., Coleman, M. L., & Love, L. G. (1986). Pore water evolution during sediment burial from isotopic and mineral chemistry of calcite, dolomite and siderite concretions. Geochimica et Cosmochimica Acta, 50(10), 2321–2334. https://doi.org/10.1016/0016-7037(86)90085-2

Dart, C. J., Bosence, D. W. J., & McClay, K. R. (1993). Stratigraphy and structure of the Maltese graben system. Journal of the Geological Society, 150(6), 1153–1166. https://doi.org/10.1144/GSJGS.150.6.1153

de la Vara, A., & Meijer, P. (2016). Response of Mediterranean circulation to Miocene shoaling and closure of the Indian Gateway: A model study. Palaeogeography, Palaeoclimatology, Palaeoecology, 442, 96–109. https://doi.org/10.1016/J.PALAEO.2015.11.002

Dijkstra, N., Kraal, P., Kuypers, M. M. M., Schnetger, B., & Slomp, C. P. (2014). Are Iron-Phosphate Minerals a Sink for Phosphorus in Anoxic Black Sea Sediments? PLOS ONE, 9(7), e101139. https://doi.org/10.1371/JOURNAL.PONE.0101139

Drake, N. A., Blench, R. M., Armitage, S. J., Bristow, C. S., & White, K. H. (2011). Ancient watercourses and biogeography of the Sahara explain the peopling of the desert. Proceedings of the National Academy of Sciences of the United States of America, 108(2), 458–462. https://doi.org/10.1073/PNAS.1012231108

Drake, N. A., Candy, I., Breeze, P., Armitage, S. J., Gasmi, N., Schwenninger, J. L., Peat, D., & Manning, K. (2022). Sedimentary and geomorphic evidence of Saharan megalakes: A synthesis. Quaternary Science Reviews, 276, 107318. https://doi.org/10.1016/J.QUASCIREV.2021.107318

Eaton, S., & Robertson, A. (1993). The Miocene Pakhna Formation, southern Cyprus and its relationship to the Neogene tectonic evolution of the Eastern Mediterranean. Sedimentary Geology, 86(3–4), 273–296. https://doi.org/10.1016/0037-0738(93)90026-2

Emerson, D. (2016). The irony of iron - Biogenic iron oxides as an iron source to the ocean. Frontiers in Microbiology, 6(JAN), 174190. https://doi.org/10.3389/FMICB.2015.01502/BIBTEX

Essid, J., Saidi, R., Ahmed, A. H., Felhi, M., Fattah, N., & Tlili, A. (2019). Characterization, nomenclature and factors controlling the stability of quartz and opal-CT of Burdigalian and Ypresian siliceous rocks from Tunisia. Journal of African Earth Sciences, 155, 151–160. https://doi.org/10.1016/j.jafrearsci.2019.04.018

Filippelli, G. M., Sierro, F. J., Flores, J. A., Vázquez, A., Utrilla, R., Pérez-Folgado, M., & Latimer, J. C. (2003). A sediment–nutrient–oxygen feedback responsible for productivity variations in Late Miocene sapropel sequences of the western Mediterranean. Palaeogeography, Palaeoclimatology, Palaeoecology, 190, 335–348. https://doi.org/10.1016/S0031-0182(02)00613-2

Filippidi, A., & Lange, G. J. De. (2019). Eastern Mediterranean Deep Water Formation During Sapropel S1: A Reconstruction Using Geochemical Records Along a Bathymetric Transect in the Adriatic Outflow Region. Paleoceanography and Paleoclimatology, 34(3), 409–429. https://doi.org/10.1029/2018PA003459

Filippidi, A., Triantaphyllou, M. V., & De Lange, G. J. (2016). Eastern-Mediterranean ventilation variability during sapropel S1 formation, evaluated at two sites influenced by deep-water formation from Adriatic and Aegean Seas. Quaternary Science Reviews, 144, 95–106.

Föllmi, K. B., Gertsch, B., Renevey, J.-P., De Kaenel, E., & Stille, P. (2008). Stratigraphy and sedimentology of phosphate-rich sediments in Malta and south-eastern Sicily (latest Oligocene to early Late Miocene). Sedimentology, 55(4), 1029–1051. https://doi.org/10.1111/j.1365-3091.2007.00935.x

Frost, B. W., & Franzen, N. C. (1992). Grazing and iron limitation in the control of phytoplankton stock and nutrient concentration: a chemostat analogue of the Pacific equatorial upwelling zone. MARINE ECOLOGY PROGRESS SERIES Mar. Ecol. Prog. Ser, 83, 291–303.

Gradstein, F. M., Ogg, J. G., Schmitz, M. D., & Ogg, G. (2020). Geologic time scale 2020. https://doi.org/10.1016/C2020-1-02369-3

Grant, K. M., Grimm, R., Mikolajewicz, U., Marino, G., Ziegler, M., & Rohling, E. J. (2016). The timing of Mediterranean sapropel deposition relative to insolation, sea-level and African monsoon changes. Quaternary Science Reviews, 140, 125–141. https://doi.org/10.1016/J.QUASCIREV.2016.03.026

Haq, B., Gorini, C., Baur, J., Moneron, J., & Rubino, J. L. (2020). Deep Mediterranean's Messinian evaporite giant: How much salt? Global and Planetary Change, 184, 103052. https://doi.org/10.1016/J.GLOPLACHA.2019.103052

Herut, B., Collier, R., & Krom, M. D. (2002). The role of dust in supplying nitrogen and phosphorus to the Southeast Mediterranean. Limnology and Oceanography, 47(3), 870–878. https://doi.org/10.4319/LO.2002.47.3.0870

Higgins, J. A., Blättler, C. L., Lundstrom, E. A., Santiago-Ramos, D. P., Akhtar, A. A., Crüger Ahm, A. S., Bialik, O., Holmden, C., Bradbury, H., Murray, S. T., & Swart, P. K. (2018). Mineralogy, early marine diagenesis,

and the chemistry of shallow-water carbonate sediments. Geochimica et Cosmochimica Acta, 220, 512–534. https://doi.org/10.1016/J.GCA.2017.09.046

Hounslow, M. W., White, H. E., Drake, N. A., Salem, M. J., El-Hawat, A., McLaren, S. J., Karloukovski, V., Noble, S. R., & Hlal, O. (2017). Miocene humid intervals and establishment of drainage networks by 23 Ma in the central Sahara, southern Libya. Gondwana Research, 45, 118–137. https://doi.org/10.1016/J.GR.2016.11.008

Hüneke, H., & Henrich, R. (2011). Pelagic Sedimentation in Modern and Ancient Oceans. Developments in Sedimentology, 63(C), 215–351. https://doi.org/10.1016/B978-0-444-53000-4.00004-4

Hutchins, D. A., Hare, C. E., Weaver, R. S., Zhang, Y., Firme, G. F., DiTullio, G. R., Alm, M. B., Riseman, S. F., Maucher, J. M., Geesey, M. E., Trick, C. G., Smith, G. J., Rue, E. L., Conn, J., & Bruland, K. W. (2002). Phytoplankton iron limitation in the Humboldt Current and Peru Upwelling. Limnology and Oceanography, 47(4), 997–1011. https://doi.org/10.4319/LO.2002.47.4.0997

Immenhauser, A. (2022). On the delimitation of the carbonate burial realm. The Depositional Record, 8(2), 524–574. https://doi.org/10.1002/DEP2.173

Incarbona, A., & Sprovieri, M. (2020). The Postglacial Isotopic Record of Intermediate Water Connects Mediterranean Sapropels and Organic-Rich Layers. Paleoceanography and Paleoclimatology, 35(10), e2020PA004009. https://doi.org/10.1029/2020PA004009

Influence of rock composition on kinetics of silica phase changes in the Monterey Formation, Santa Barbara area, California | Geology | GeoScienceWorld. (n.d.). Retrieved December 2, 2024, from https://pubs.geoscienceworld.org/gsa/geology/article-abstract/10/6/304/190848/Influence-of-rock-composition-on-kinetics-of?redirectedFrom=fulltext

Jacobs, E., Weissert, H., Shields, G., & Stille, P. (1996). The monterey event in the Mediterranean: A record from shelf sediments of Malta. Paleoceanography, 11(6). https://doi.org/10.1029/96PA02230

Jiang, H. B., Hutchins, D. A., Ma, W., Zhang, R. F., Wells, M., Jiao, N., Wang, Y., & Chai, F. (2023). Natural ocean iron fertilization and climate variability over geological periods. Global Change Biology, 29(24), 6856–6866. https://doi.org/10.1111/GCB.16990

Jickells, T., & Moore, C. M. (2015). The Importance of Atmospheric Deposition for Ocean Productivity. Annual Review of Ecology, Evolution, and Systematics, 46(Volume 46, 2015), 481–501. https://doi.org/10.1146/ANNUREV-ECOLSYS-112414-054118/CITE/REFWORKS

John, C. M., Mutti, M., & Adatte, T. (2003). Mixed carbonate-siliciclastic record on the North African margin (Malta) - coupling of weathering processes and mid Miocene climate. Geological Society of America Bulletin, 115(2), 217–229. https://doi.org/10.1130/0016-7606(2003)115<0217:MCSROT>2.0.CO;2

Karpoff, A. M., Destrigneville, C., & Stille, P. (2007). Clinoptilolite as a new proxy of enhanced biogenic silica productivity in lower Miocene carbonate sediments of the Bahamas platform: Isotopic and thermodynamic evidence. Chemical Geology, 245(3–4), 285–304. https://doi.org/10.1016/J.CHEMGEO.2007.08.011

Kidd, R., Rb, K., Cita, M., & Wbf, R. (1978). Stratigraphy of Eastern Mediterranean sapropel sequences recovered during DSDP Leg 42a and their paleoenvironmental significance. Initial Reports of the Deep Sea Drilling Project, 42 Pt. 1. https://doi.org/10.2973/DSDP.PROC.42-1.113-1.1978

Kocken, I. J., Cramwinckel, M. J., Zeebe, R. E., Middelburg, V. J., & Sluijs, A. (2019). The 405 kyr and 2.4 Myr eccentricity components in Cenozoic carbon isotope records. Climate of the Past, 15(1), 91–104. https://doi.org/10.5194/CP-15-91-2019

Leonova, G. A., Maltsev, A. E., Melenevsky, V. N., Krivonogov, S. K., Kondratyeva, L. M., Bobrov, V. A., & Suslova, M. Y. (2019). Diagenetic transformation of organic matter in sapropel sediments of small lakes (southern West Siberia and eastern Transbaikalia). Quaternary International, 524, 40–47. https://doi.org/10.1016/J.QUAINT.2019.03.011

Li, C., Dong, L., Ma, H., Liu, H., Li, C., Pei, H., & Shen, B. (2022). Formation of the massive bedded chert and coupled Silicon and Iron cycles during the Ediacaran-Cambrian transition. Earth and Planetary Science Letters, 594, 117721. https://doi.org/10.1016/J.EPSL.2022.117721

Lyu, J., Auer, G., Bialik, O. M., Christensen, B., Yamaoka, R., & De Vleeschouwer, D. (2023). Astronomically-Paced Changes in Paleoproductivity, Winnowing, and Mineral Flux Over Broken Ridge (Indian Ocean) Since the Early Miocene. Paleoceanography and Paleoclimatology, 38(12), e2023PA004761. https://doi.org/10.1029/2023PA004761

Madsen, H. B., & Stemmerik, L. (2010). Diagenesis of Flint and Porcellanite in the Maastrichtian Chalk at Stevns Klint, Denmark. Journal of Sedimentary Research, 80(6), 578–588. https://doi.org/10.2110/jsr.2010.052

Maliva, R. G., Knoll, A. H., & Simonson, B. M. (2005). Secular change in the Precambrian silica cycle: Insights from chert petrology. GSA Bulletin, 117(7–8), 835–845. https://doi.org/10.1130/B25555.1

Maliva, R. G., & Siever, R. (1989). Nodular Chert Formation in Carbonate Rocks. Source: The Journal of Geology, 97(4), 421–433. https://www.jstor.org/stable/30078348

Mancini, A. M., Bocci, G., Morigi, C., Gennari, R., Lozar, F., & Negri, A. (2023). Past Analogues of Deoxygenation Events in the Mediterranean Sea: A Tool to Constrain Future Impacts. Journal of Marine Science and Engineering, 11(3), 562. https://doi.org/10.3390/JMSE11030562/S1

Martin, J. H. (1990). Glacial-interglacial CO2 change: The Iron Hypothesis. Paleoceanography, 5(1), 1–13. https://doi.org/10.1029/PA005I001P00001

McCrea, J. M. (1950). On the Isotopic Chemistry of Carbonates and a Paleotemperature Scale. The Journal of Chemical Physics, 18(6), 849–857. https://doi.org/10.1063/1.1747785

Meijer, P. (2021). (Paleo)oceanography of semi-enclosed seas with a focus on the Mediterranean region; Insights from basic theory. Earth-Science Reviews, 221, 103810. https://doi.org/10.1016/J.EARSCIREV.2021.103810

Meister, P., Herda, G., Petrishcheva, E., Gier, S., Dickens, G. R., Bauer, C., & Liu, B. (2022). Microbial Alkalinity Production and Silicate Alteration in Methane Charged Marine Sediments: Implications for Porewater Chemistry and Diagenetic Carbonate Formation. Frontiers in Earth Science, 9, 756591. https://doi.org/10.3389/FEART.2021.756591/BIBTEX

Meyer, K. M., & Kump, L. R. (2008). Oceanic euxinia in Earth history: Causes and consequences. Annual Review of Earth and Planetary Sciences, 36(Volume 36, 2008), 251–288. https://doi.org/10.1146/ANNUREV.EARTH.36.031207.124256/CITE/REFWORKS

Miller, K. G., Browning, J. V., Schmelz, W. J., Kopp, R. E., Mountain, G. S., & Wright, J. D. (2020). Cenozoic sea-level and cryospheric evolution from deep-sea geochemical and continental margin records. Science Advances, 6(20), eaaz1346. https://doi.org/10.1126/sciadv.aaz1346

Mourik, A. A., Abels, H. A., Hilgen, F. J., Di Stefano, A., & Zachariasse, W. J. (2011). Improved astronomical age constraints for the middle Miocene climate transition based on high-resolution stable isotope records from the central Mediterranean Maltese Islands. Paleoceanography, 26(1). https://doi.org/10.1029/2010PA001981

Ohfuji, H., & Rickard, D. (2005). Experimental syntheses of framboids—a review. Earth-Science Reviews, 71(3–4), 147–170. https://doi.org/10.1016/J.EARSCIREV.2005.02.001

Online, G., & Malaysian, T. M. (2021). Calcareous nannofloras in Western Lobe Offshore, Niger Delta: Eutrophication and climate change implications. Journal of Society and Space, 17(4), 274–287. https://doi.org/10.17576/geo-2021-1704-19

Oren, O. H. (1969). Oceanographic and biological influence of the Suez Canal, the Nile and the Aswan Dam on the Levant Basin. Progress in Oceanography, 5(C), 161–167. https://doi.org/10.1016/0079-6611(69)90038-X

Oretade, B. S. (2021). Calcareous nannofloras in Western Lobe Offshore, Niger Delta : eutrophication and climate change implications.

Passier, H. F., & De Lange, G. J. (1998). Sedimentary sulfur and iron chemistry in relation to the formation of eastern Mediterranean sapropels. Proceedings of the Ocean Drilling Program: Scientific Results, 160, 249–260. https://doi.org/10.2973/ODP.PROC.SR.160.020.1998

Pedley, H. M., House, M. R., & Waugh, B. (1978). The Geology of the Pelagian Block: The Maltese Islands. The Ocean Basins and Margins, 417–433. https://doi.org/10.1007/978-1-4684-3039-4_8

Pedley, M. (1996). Miocene Reef Facies of the Pelagian Region (Central Mediterranean). Models for Carbonate Stratigraphy from Miocene Reef Complexes of Mediterranean Regions: https://doi.org/10.2110/csp.96.01.0247

Pérez-Asensio, J. N., Frigola, J., Pena, L. D., Sierro, F. J., Reguera, M. I., Rodríguez-Tovar, F. J., Dorador, J., Asioli, A., Kuhlmann, J., Huhn, K., & Cacho, I. (2020). Changes in western Mediterranean thermohaline circulation in association with a deglacial Organic Rich Layer formation in the Alboran Sea. Quaternary Science Reviews, 228, 106075. https://doi.org/10.1016/J.QUASCIREV.2019.106075

Petrash, D. A., Bialik, O. M., Bontognali, T. R. R., Vasconcelos, C., Roberts, J. A., McKenzie, J. A., & Konhauser, K. O. (2017). Microbially catalyzed dolomite formation: From near-surface to burial. Earth-Science Reviews, 171, 558–582. https://doi.org/10.1016/J.EARSCIREV.2017.06.015

Petrash, D. A., Bialik, O. M., Staudigel, P. T., Konhauser, K. O., & Budd, D. A. (2021). Biogeochemical reappraisal of the freshwater–seawater mixing-zone diagenetic model. Sedimentology, 68(5), 1797–1830. https://doi.org/10.1111/SED.12849

Petrash, D. A., Robbins, L. J., Shapiro, R. S., Mojzsis, S. J., & Konhauser, K. O. (2016). Chemical and textural overprinting of ancient stromatolites: Timing, processes, and implications for their use as paleoenvironmental proxies. Precambrian Research, 278, 145–160. https://doi.org/10.1016/J.PRECAMRES.2016.03.010

Petrash, D. A., Steenbergen, I. M., Valero, A., Meador, T. B., Paces, T., & Thomazo, C. (2022). Aqueous system-level processes and prokaryote assemblages in the ferruginous and sulfate-rich bottom waters of a post-mining lake. Biogeosciences, 19(6), 1723–1751. https://doi.org/10.5194/BG-19-1723-2022

Poulton, S. W., & Canfield, D. E. (2005). Development of a sequential extraction procedure for iron: implications for iron partitioning in continentally derived particulates. Chemical Geology, 214(3–4), 209–221. https://doi.org/10.1016/J.CHEMGEO.2004.09.003

Raiswell, R., & Canfield, D. E. (1998). Sources of iron for pyrite formation in marine sediments. American Journal of Science, 298(3), 219–245. https://doi.org/10.2475/AJS.298.3.219

Reich, T., Ben-Ezra, T., Belkin, N., Tsemel, A., Aharonovich, D., Roth-Rosenberg, D., Givati, S., Bialik, M., Herut, B., Berman-Frank, I., Frada, M., Krom, M. D., Lehahn, Y., Rahav, E., & Sher, D. (2022). A year in the life of the Eastern Mediterranean: Monthly dynamics of phytoplankton and bacterioplankton in an ultra-oligotrophic sea. Deep Sea Research Part I: Oceanographic Research Papers, 182, 103720. https://doi.org/10.1016/J.DSR.2022.103720

Riahi, S., Soussi, M., & Ben Ismail Lattrache, K. (2015). Age, internal stratigraphic architecture and structural style of the oligocene-miocene numidian formation of northern Tunisia. Annales Societatis Geologorum Poloniae, 85(2), 345–370. https://doi.org/10.14241/ASGP.2015.009

Rickard, D. (2019). Sedimentary pyrite framboid size-frequency distributions: A meta-analysis. https://doi.org/10.1016/j.palaeo.2019.03.010

Rögl, F. (1999). Mediterranean and Paratethys. Facts and hypotheses of an Oligocene to Miocene paleogeography (short overview). Geologica Carpathica 50-4, 339–349.

Rohling, E. J. (1994). Review and new aspects concerning the formation of eastern Mediterranean sapropels. Marine Geology, 122(1–2), 1–28.

Rohling, E. J., Marino, G., & Grant, K. M. (2015). Mediterranean climate and oceanography, and the periodic development of anoxic events (sapropels). Earth-Science Reviews, 143, 62–97. https://doi.org/10.1016/J.EARSCIREV.2015.01.008

Rosenbaum, J., & Sheppard, S. M. F. (1986). An isotopic study of siderites, dolomites and ankerites at high temperatures. Geochimica et Cosmochimica Acta, 50(6), 1147–1150. https://doi.org/10.1016/0016-7037(86)90396-0

Roveri, M., Lugli, S., Manzi, V., Reghizzi, M., & Rossi, F. P. (2020). Stratigraphic relationships between shallow-water carbonates and primary gypsum: insights from the Messinian succession of the Sorbas Basin (Betic Cordillera, Southern Spain). Sedimentary Geology, 404, 105678. https://doi.org/10.1016/J.SEDGEO.2020.105678

Rubin-Blum, M., Antler, G., Turchyn, A. V., Tsadok, R., Goodman-Tchernov, B. N., Shemesh, E., Austin, J. A., Coleman, D. F., Makovsky, Y., Sivan, O., & Tchernov, D. (2014). Hydrocarbon-related microbial processes in the deep sediments of the Eastern Mediterranean Levantine Basin. FEMS Microbiology Ecology, 87(3), 780–796. https://doi.org/10.1111/1574-6941.12264

Rutten, A., De Lange, G. J., Hayes, A., Rohling, E. J., De Jong, A. F. M., & Van Der Borg, K. (1999). Deposition of sapropel S1 sediments in oxic pelagic and anoxic brine environments in the eastern Mediterranean: differences in diagenesis and preservation. Marine Geology, 153(1–4), 319–335. https://doi.org/10.1016/S0025-3227(98)00076-0

Sela-Adler, M., Herut, B., Bar-Or, I., Antler, G., Eliani-Russak, E., Levy, E., Makovsky, Y., & Sivan, O. (2015). Geochemical evidence for biogenic methane production and consumption in the shallow sediments of the SE Mediterranean shelf (Israel). Continental Shelf Research, 101, 117–124. https://doi.org/10.1016/J.CSR.2015.04.001

Sibert, E. C., & Rubin, L. D. (2021). An early Miocene extinction in pelagic sharks. Science, 372(6546), 1105–1107. https://doi.org/10.1126/SCIENCE.AAZ3549/

Sinninghe Damst'e, J. S., Rijpstra, W. I. C., Kock-van Dalen, A. C., De Leeuw, J. W., & Schenck, P. A. (1989). Quenching of labile functionalised lipids by inorganic sulphur species: Evidence for the formation of sedimentary organic sulphur compounds at the early stages of diagenesis. Geochimica et Cosmochimica Acta, 53(6), 1343–1355. https://doi.org/10.1016/0016-7037(89)90067-7

Sigl W., Chamley H., Fabricus F., Giroud d'Argoud G., Muller, J. (1978) Sedimentology and conditions of sapropels. Deep Sea Drilling Project Initial Reports Volume 42, part 1.

Sisma-Ventura, G., Bialik, O. M., Makovsky, Y., Rahav, E., Ozer, T., Kanari, M., Marmen, S., Belkin, N., Guy-Haim, T., Antler, G., Herut, B., & Rubin-Blum, M. (2022). Cold seeps alter the near-bottom biogeochemistry in the ultraoligotrophic Southeastern Mediterranean Sea. Deep Sea Research Part I: Oceanographic Research Papers, 183, 103744. https://doi.org/10.1016/J.DSR.2022.103744

Taylforth, J. E., McCay, G. A., Ellam, R., Raffi, I., Kroon, D., & Robertson, A. H. F. (2014). Middle Miocene (Langhian) sapropel formation in the easternmost Mediterranean deep-water basin: Evidence from northern Cyprus. Marine and Petroleum Geology, 57, 521–536. https://doi.org/10.1016/J.MARPETGEO.2014.04.015

Thomson, J., Crudeli, D., De Lange, G. J., Slomp, C. P., Erba, E., Corselli, C., & Calvert, S. E. (2004). Florisphaera profunda and the origin and diagenesis of carbonate phases in eastern Mediterranean sapropel units. Paleoceanography, 19(3). https://doi.org/10.1029/2003PA000976

Urban, N. R., Ernst, K., & Bernasconi, S. (1999). Addition of sulfur to organic matter during early diagenesis of lake sediments. Geochimica et Cosmochimica Acta, 63(6), 837–853. https://doi.org/10.1016/S0016-7037(98)00306-8

Watson, A. J., Bakker, D. C. E., Ridgwell, A. J., Boyd, P. W., & Law, C. S. (2000). Effect of iron supply on Southern Ocean CO2 uptake and implications for glacial atmospheric CO2. Nature 2000 407:6805, 407(6805), 730–733. https://doi.org/10.1038/35037561

Westerhold, T., Marwan, N., Drury, A. J., Liebrand, D., Agnini, C., Anagnostou, E., Barnet, J. S. K., Bohaty, S. M., De Vleeschouwer, D., Florindo, F., Frederichs, T., Hodell, D. A., Holbourn, A. E., Kroon, D., Lauretano, V., Littler, K., Lourens, L. J., Lyle, M., Pälike, H., … Zachos, J. C. (2020). An astronomically dated record of Earth's climate and its predictability over the last 66 million years. Science (New York, N.Y.), 369(6509), 1383–1388. https://doi.org/10.1126/SCIENCE.ABA6853

Wilkin, R. T., Arthur, M. A., & Dean, W. E. (1997). History of water-column anoxia in the Black Sea indicated by pyrite framboid size distributions. Earth and Planetary Science Letters, 148(3–4), 517–525. https://doi.org/10.1016/S0012-821X(97)00053-8

Wilkin, R. T., Barnes, H. L., & Brantley, S. L. (1996). The size distribution of framboidal pyrite in modern sediments: An indicator of redox conditions. Geochimica et Cosmochimica Acta, 60(20), 3897–3912. https://doi.org/10.1016/0016-7037(96)00209-8

Wignall, P. B., & Newton, R. (1998). Pyrite framboid diameter as a measure of oxygen deficiency in ancient mudrocks. *American Journal of Science*, *298*(7), 537-552.

Woods, T. L., & Garrels, R. M. (1992). Calculated aqueous-solution-solid-solution relations in the low-temperature system CaO-MgO-FeO-CO2-H2O. Geochimica et Cosmochimica Acta, 56(8), 3031–3043. https://doi.org/10.1016/0016-7037(92)90288-T

Wu, C. H., Lee, S. Y., & Tsai, P. C. (2021). Role of eccentricity in early Holocene African and Asian summer monsoons. Scientific Reports 2021 11:1, 11(1), 1–13. https://doi.org/10.1038/s41598-021-03525-z

Wurgaft, E., Findlay, A. J., Vigderovich, H., Herut, B., & Sivan, O. (2019). Sulfate reduction rates in the sediments of the Mediterranean continental shelf inferred from combined dissolved inorganic carbon and total alkalinity profiles. Marine Chemistry, 211, 64–74. https://doi.org/10.1016/J.MARCHEM.2019.03.004

Zammit, R., Lear, C. H., Samankassou, E., Lourens, L. J., Micallef, A., Pearson, P. N., & Bialik, O. M. (2022). Early Miocene Intensification of the North African Hydrological Cycle: Multi-Proxy Evidence From the Shelf Carbonates of Malta. Paleoceanography and Paleoclimatology, 37(9). https://doi.org/10.1029/2022PA004414

Zirks, E., Krom, M. D., Zhu, D., Schmiedl, G., & Goodman-Tchernov, B. N. (2019). Evidence for the Presence of Oxygen-Depleted Sapropel Intermediate Water across the Eastern Mediterranean during Sapropel S1. ACS Earth and Space Chemistry, 3(10), 2287–2297. https://doi.org/10.1021/ACSEARTHSPACECHEM.9B00128/SUPPL_FILE/SP9B00128_SI_001.PDF

Climatic and tectonic controls on ferroan dolomite formation – insights on Early Miocene Mediterranean anoxia (il-Blata, Malta).

Ray Zammit, Daniel A. Petrash, Or M. Bialik

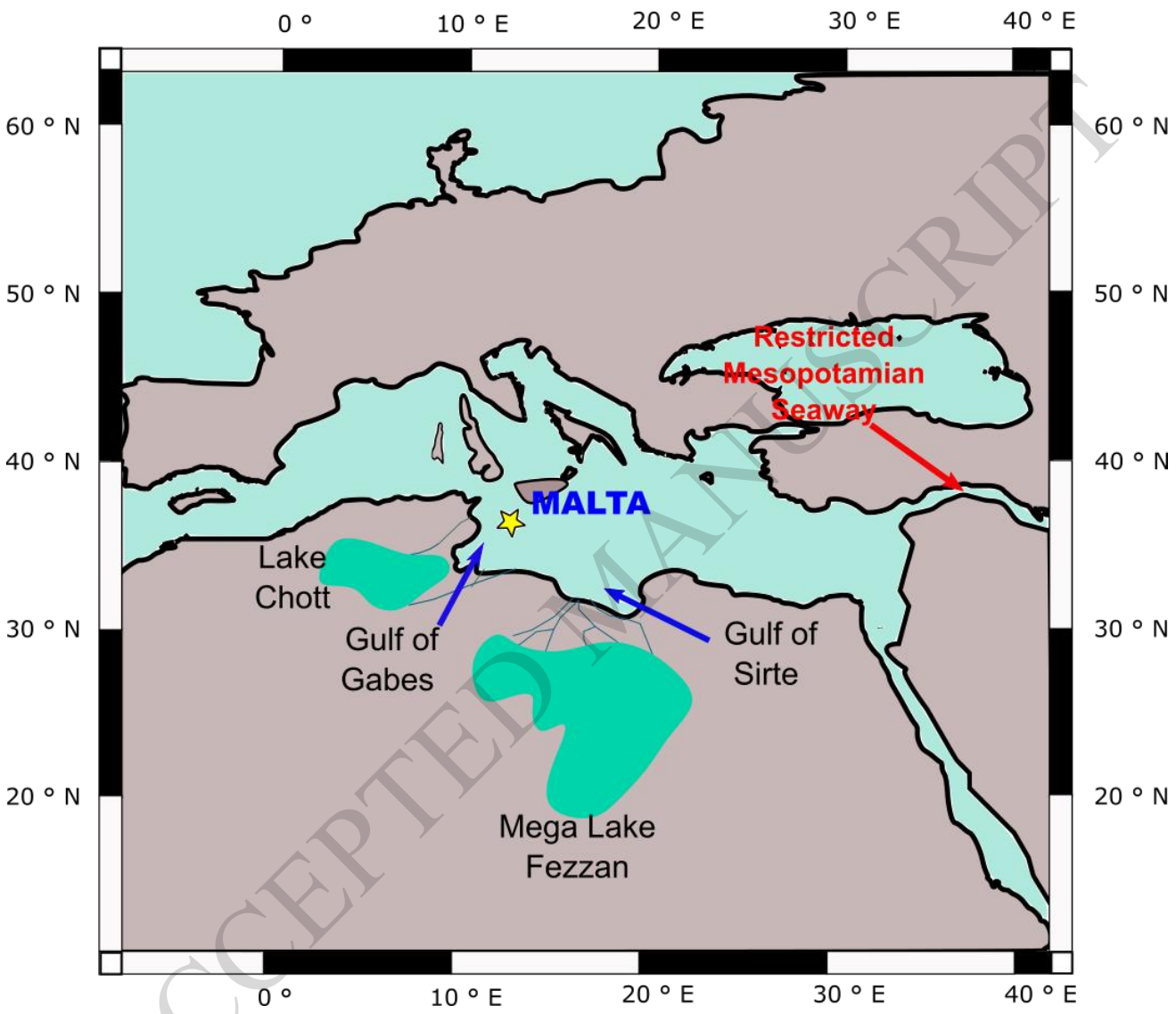

Figure 1. Around 20 Ma the Mesopotamian Seaway connecting the Mediterranean with the Indian Ocean became severely restricted due to tectonic movement of the African and Arabian plates (Bialik et. al., 2019) This configuration favoured intensified Atlantic weather resulting in a wetter western Sahara and high siliciclastic input into via continental runoff into Central Mediterranean. The mixed carbonate-siliciclastic deposits of Malta hold a record of these events.

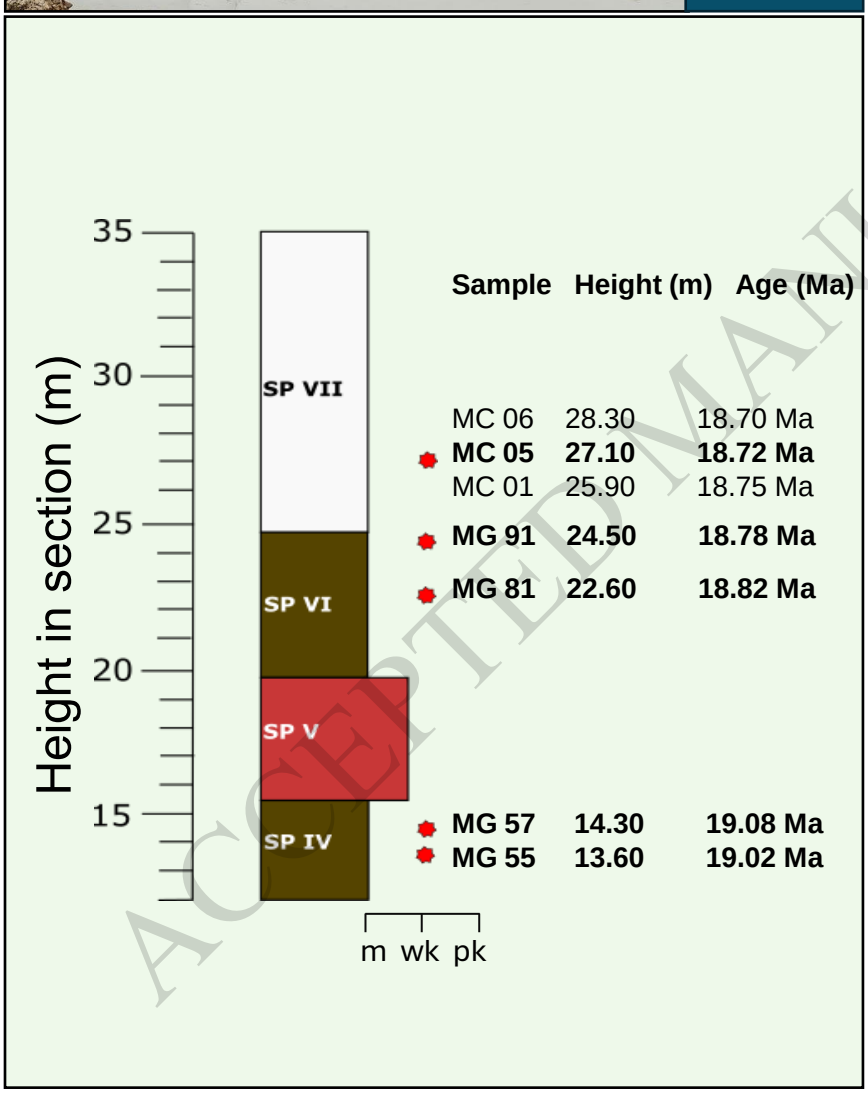

Figure 2. Il-Blata section in the Central Mediterranean Island of Malta hosts organic-rich facies superimposed by chert-rich carbonate facies of Early Miocene age. Five representative samples have been selected from the organic-rich (SP IV and SP VI) and chert-rich (SP VII) packages. Ages obtained via $^{87}Sr/^{86}Sr$ system (Zammit et. al., 2022).

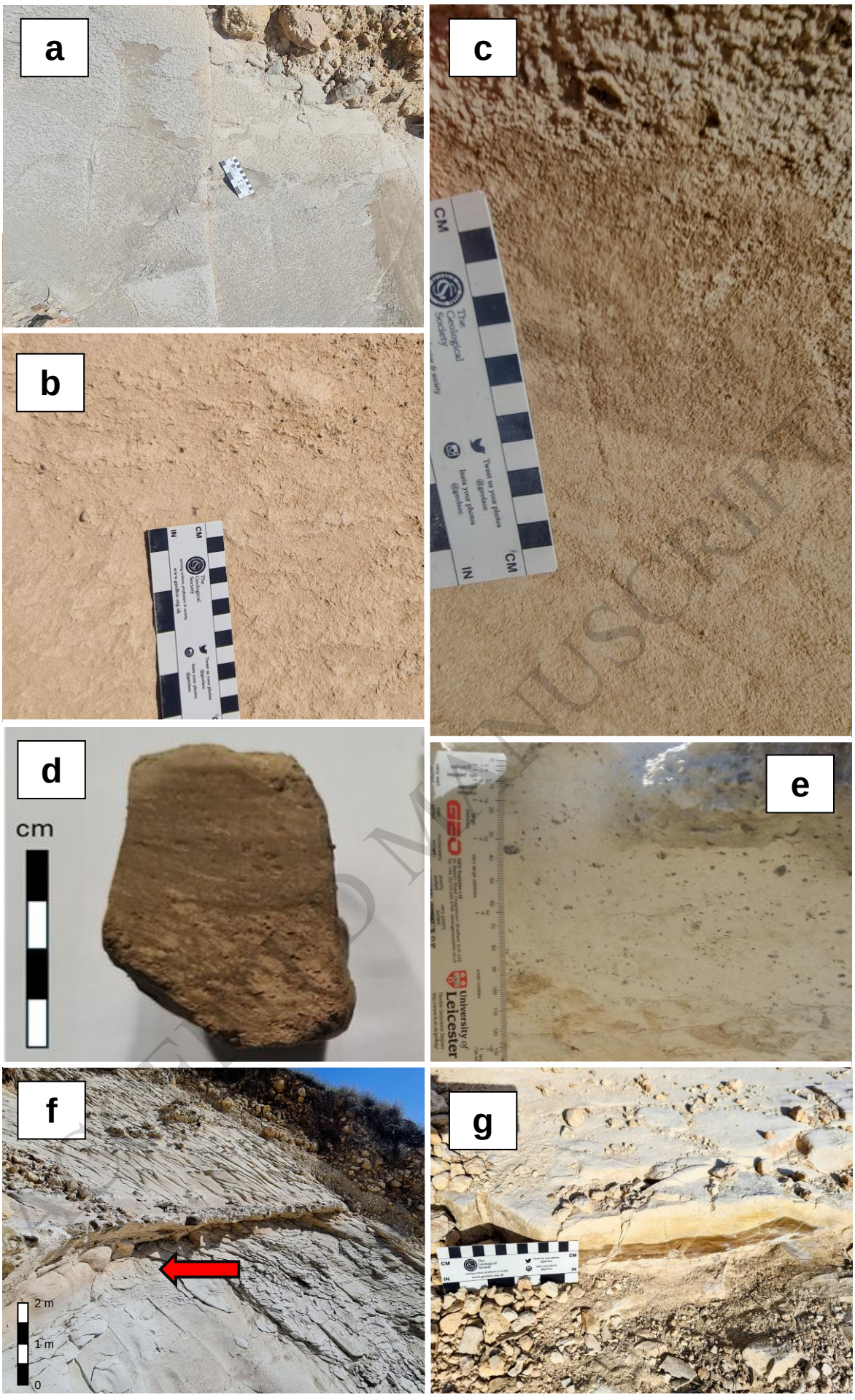

Figure 3. (a) Dark coloured mustones pertaining to SP IV, (b) centimeter sized allochthonous phosphatic pebbles within mudstone/wakestone facies of SPV (c) conformant transition from SP V mudstone/wakestone associations to dark mudstones of SP VI, (d) very finely laminated dark green to beige organic-rich mudstones of SP-VII, (e) siliceous pebbels at the base of the cherty musdstones of SP VII (f) Arrow indicating continuous sedimentation and shift from organic-rich facies of SP VI to cream coloured siliceous facies of SP VII, (g) chert nodule seen in cross-section occupying space within the muddy siliceous mudstones.

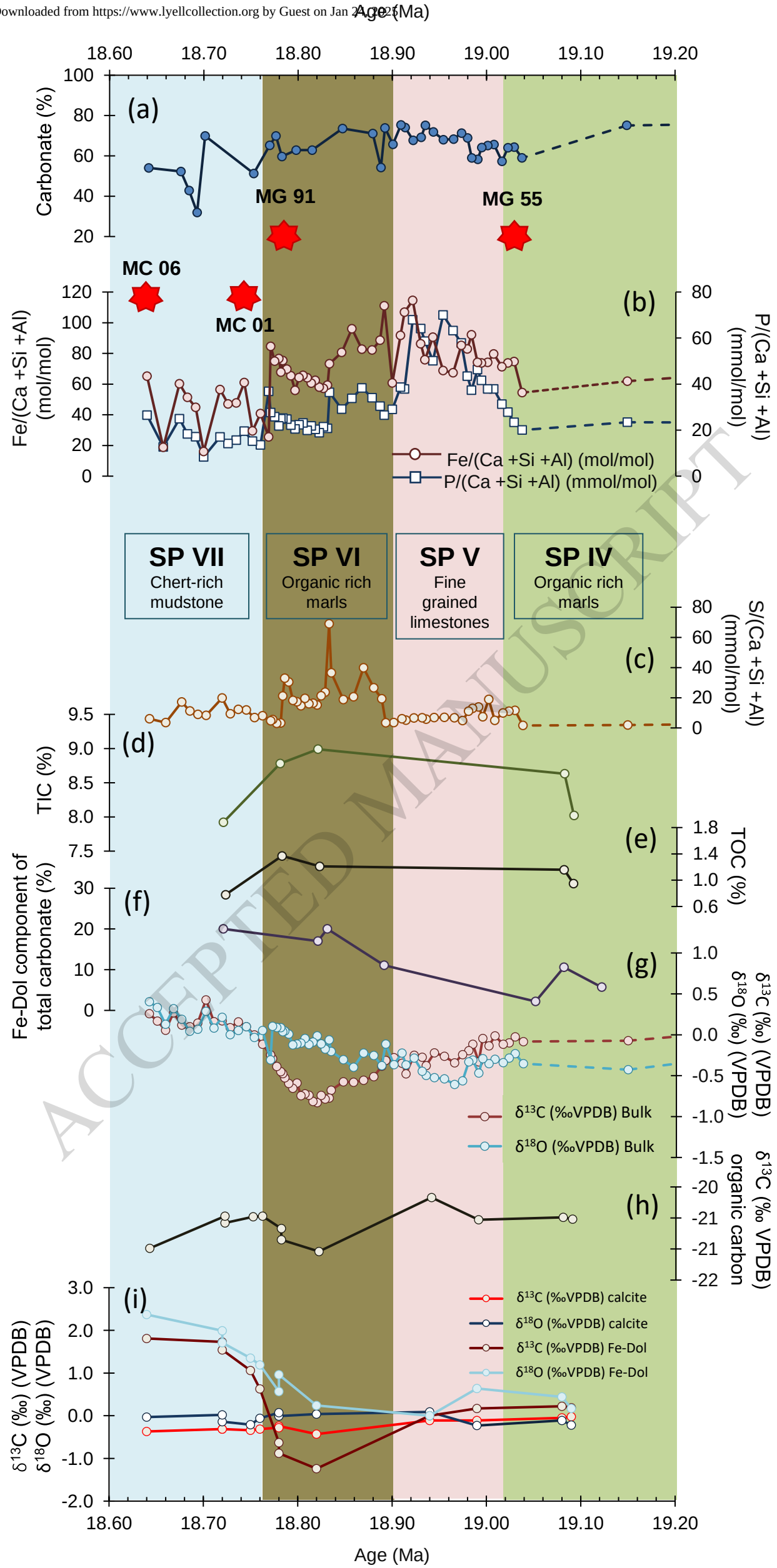

Figure 4. Bulk stable isotopes ($\delta^{18}O$ and $\delta^{13}C$) as measured on bulk sediment and on selected carbonate mineral phases. Calcite stable isotopes show little variability throughout the section while the Fe-dolomimite stable isotopes change significantly. The $\delta^{13}C$ values shift by ~ 3 ‰ as the lithology changes from the organic-rich facies of SP VI to the siliceous facies of SP VII and the $\delta^{18}O$ increase by ~ 2 ‰ for the same lithological change. The bulk $\delta^{13}C$ and the Fe-Dol $\delta^{13}C$ show decreased values associated with the organic-rich SP VI marls, a correlation not observed in the $\delta^{18}O$ records. Geochemical records highlighting the variability in the stable isotope ($\delta^{18}O$ and $\delta^{13}C$) records of the calcite, Fe-dol and C_{org} phases with changes in total organic carbon (TOC) and % component of Ferroan dolomite of the carbonate content.

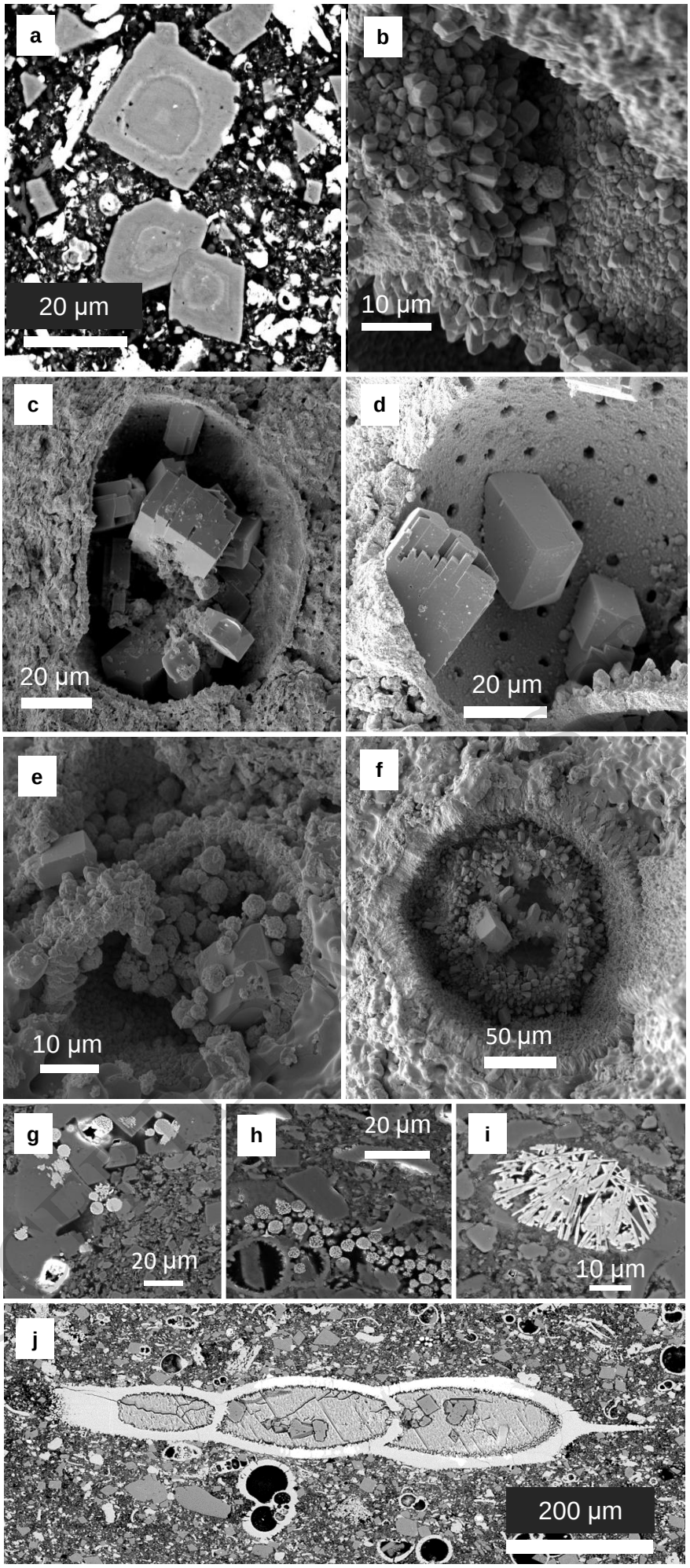

Figure 5. (a) Zoned dolomite crystals displaying Ca- and Fe- rich bands (MG 55, SP IV), (b) dolomite crystals (MG 55 SP IV), (c) blocky calcite crystals in foraminiferal test (MG 91, SP VI), (d) Inner test of well-preserved planktic foraminifera containing blocky calcite crystals (MC 01, SP VII), (e) lepisphere-like forms and calcite crystals inside re-crystallised foraminiferal test (MC 06, SP VII), (f) bacterial activity in the form of mucilage strings inside dolotomised foraminiferal test (MG 55, SP IV) (g) Large framboids ~10 um (MG 91 , SP VI) (h) small framboids within matrix (MC 06 , SP VII) (i) microcrystalline fibrous gypsum filling benthic foraminifera (MG 91 , SP VI) (j) Gypsum and calcite cement inside elongate benthic foraminifera (MC 06, SP VII).

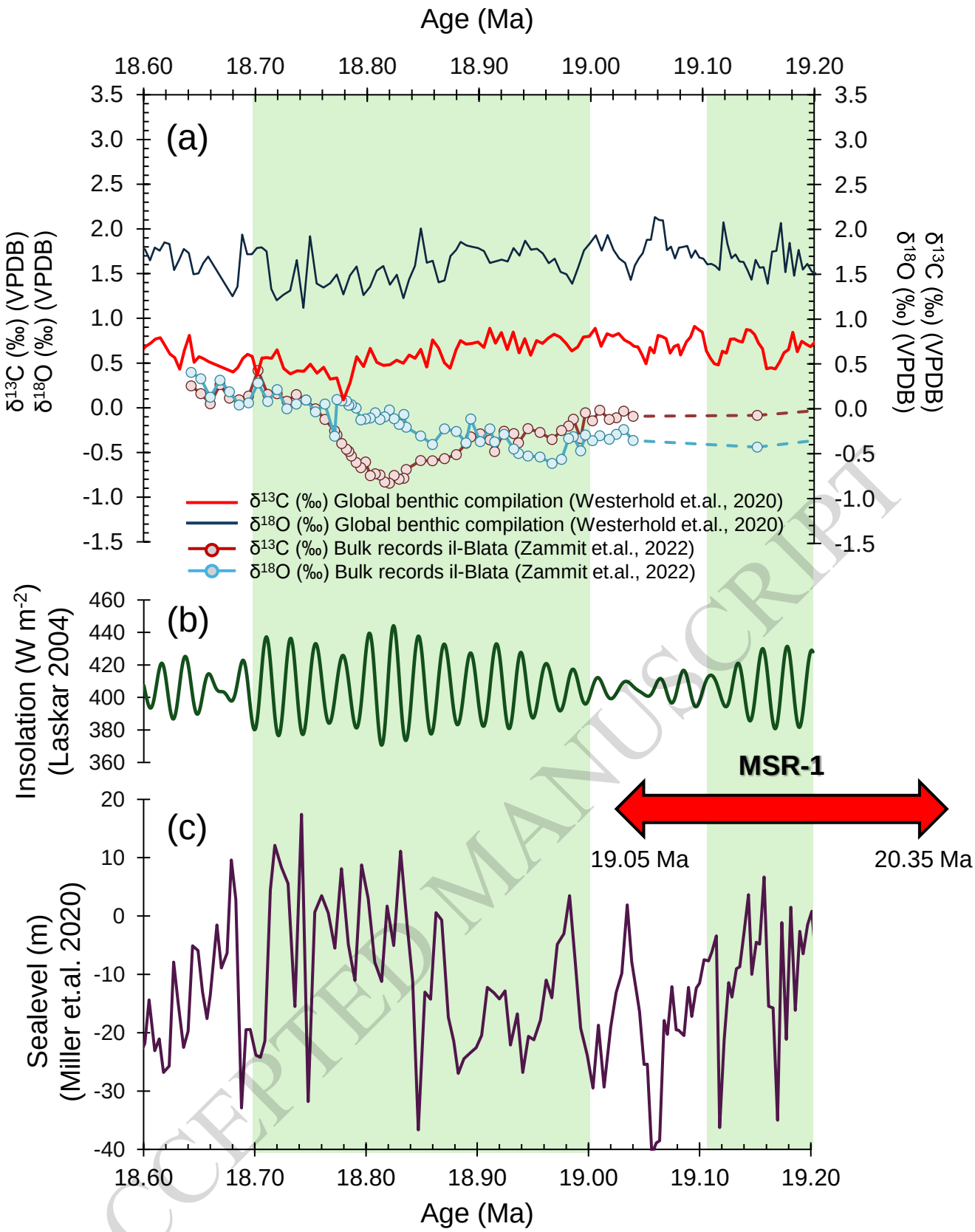

Figure 6. (a) Global benthic and bulk il-Blata carbonate stable isotope records. The bulk il-Blata $\delta^{13}C$ records demonstrate a notable negative shift in the organic-rich facies of SP VI. This is concomitant with a peak in the insolation variability (~400 kyr cycle) (b) and occurs around a trough in global sea-level (c). Rising sea-level may be associated with the positive shift in the stable isotope records and the emplacement of siliceous deposits. The MSR-1 seaway restriction occurs between 20.35 Ma and 19.05 M, coinciding with a trough in global sea-level (Zammit et.al., 2022).

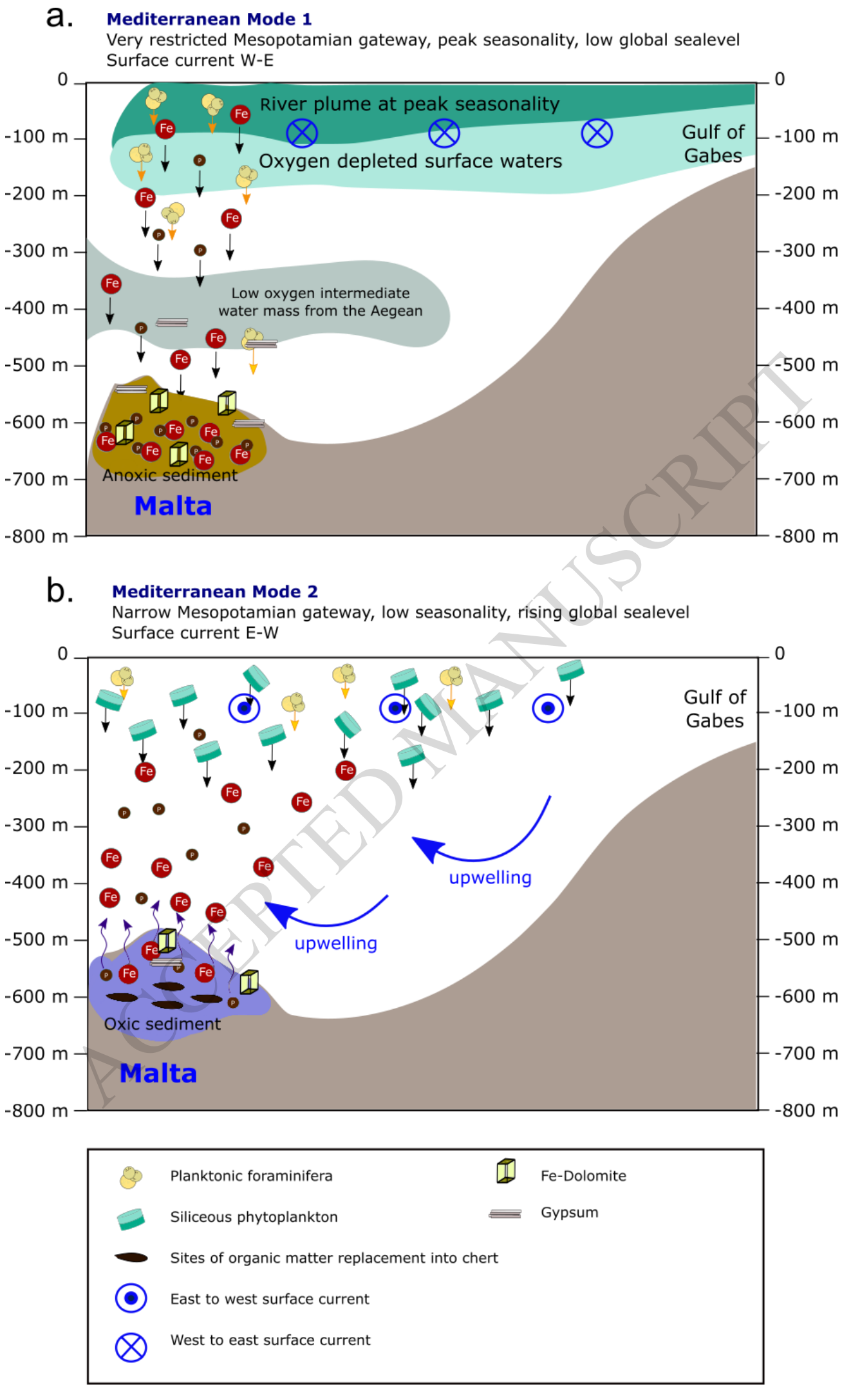

Figure 7. (a) With a heavily restricted Mesopotamian Gateway surface waters flow towards the east and help carry river plumes from the Gulf of Gabes over Malta. The closed gateway also favour intense hydroclimatic activity over western Sahara with a large plume extending into the central Mediterranean during peak insolation variability. In combination with low oxygen intermediate waters coming from the Aegean this generates anoxic conditions in the region. (b) A re-opened Mesopotamian gateway helps to restore vertical mixing, re-oxygenating the sediment and releasing iron and phosphorous into the water column. This also activates upwelling and results in a siliceous phytoplankton bloom. Silica is lithified in sites of oxidized organic matter resulting in the formation of nodular cherts.